STATUS QUO: AIR QUALITY TREND ANALYSIS REPORT FOR EZAMOKUHLE

Document by:

ARM
AIR RESOURCE MANAGEMENT

Final Report

17 February 2021

Document Title

Client	**Eskom**
Title	**Status Quo: Air Quality Trend Analysis Report for Ezamokuhle**
Our Reference	**ESKPMV-2021-ACTV-01-SQ01**
Issued to Client	**17/02/2021**
Classification	**Company Confidential**

Document Change Record

Revision Number	Date	Description of Revision
00A	1st February 2021	Creation of Document
00B	11th February 2021	Peer Review of Document
01	17th February 2021	Approval of Revised Document

Document Approval

	Name	Designation	Date
Prepared by	Mr A Shamu	Air Quality Specialist	1st February 2021
Reviewed by	Mr F Goede	Executive Head: Air Quality	11th February 2021
Approved by	Mr F Goede	Executive Head: Air Quality	17th February 2021

Contents

LIST OF TABLES

LIST OF FIGURES

EXECUTIVE SUMMARY

This study performed an analysis of trends, correlations and general relations which were based on collected ambient air quality measurement data obtained from the: Eskom Ezamokuhle Station (the *in-situ* station), Sasol Amersfoort Station (adjacent to Ezamokuhle), and the Eskom Majuba Station (the industrial station). The Openair model was utilised to statistically analyse the semi-empirical mathematical relationships between air pollutant concentrations and meteorological parameters for these three stations. Additionally the study examined the trans-boundary movement & deposition of pollutants in the Ezamokuhle airshed.

For the Eskom Ezamokuhle station, the highest NO_2 concentrations occur under very low wind speed conditions from the south-west. These high concentrations occur under stable atmospheric conditions when non-buoyant ground-level sources are important. The time variation plot at Ezamokuhle explicitly reveals that the variability of NO_2 concentrations are conditioned by vehicle emissions. For the Eskom Majuba station, NO_2 concentrations increase at just before midday due to the break-up of an elevated inversion layer, in addition to the development of daytime convective conditions causing the plume to be brought down to ground level relatively close to the point of release from tall stacks. The elevated NO_2 levels in winter at the Eskom Ezamokuhle and Majuba stations demonstrate the additional contribution of residential fuel burning sources.

At the Eskom Ezamokuhle and Majuba stations, SO_2 shows a typical industrial signature with increased SO_2 concentrations at just before midday due to the rising of the inversion layer. The pollution rose for the Eskom Majuba Station shows that elevated SO_2 concentrations are present during high wind speed conditions which is further indicative of emissions from stacks rather than non-buoyant ground-level sources. Additionally the polar plot for the mean hourly SO_2 concentration observed at the Eskom Majuba Station show that the highest SO_2 concentrations occur when the wind is blowing from the north-west which is most likely due to emissions from the Eskom Majuba Power Station. The winter elevation of SO_2 shows the contribution of residential fuel burning to the ambient SO_2 concentrations at the Eskom Ezamokuhle and Majuba stations. At the Eskom Ezamokuhle station, there is a second less pronounced peak that occurs consistently throughout the entire week at 18:00. A comparison of the trend level plot for Ezamokuhle clearly indicates that the 18:00 peak occurs in winter (peaking in the months of June and July) thus indicating the impact of residential fuel burning emissions.

The bi-modal particulate matter peak for both the Eskom Ezamokuhle and Majuba stations is a typical profile for residential fuel burning. Monthly variation of particulate matter shows elevated concentrations during early winter months to early spring due to the greater contribution from domestic fuel burning, dust from uncovered soil and the lack of the settling influence of rainfall. It's noteworthy that a monthly particulate matter peak is measured at the Eskom Ezamokuhle station for the month of December. A comparison of the trend level plot for the Eskom Ezamokuhle station shows that for the year 2020, these particulate matter emissions occur between 17:00 to 21:00 with emissions peaking at 18:00 thus indicating the impact of a residential fuel burning source.

The exceedances of the hourly SO_2 NAAQS at the Eskom Ezamokuhle and Eskom Majuba stations are attributable to a bouyant elevated tall stack emission source. Conversely the particulate matter NAAQS exceedances recorded at Eskom Ezamokuhle and Eskom Majuba stations are attributable to non-bouyant residential fuel burning emission sources. There were no recorded exceedances of the hourly NO_2 NAAQS standard.

Back trajectory modelling was undertaken using the Hybrid Single-Particle Lagrangian Integrated Trajectory (HYSPLIT) model. The HYSPLIT results has shown the transboundary impact of pollutants, within a 24-hour window, air masses from far afield such as Kwa-Zulu Natal and Eswatini impact on the Ezamokuhle airshed. The pattern of the 24-hour back trajectory results correspond to the influence of a semi-permanent sub-tropical anticyclone over the Highveld region. These high pressure systems are associated with large-scale subsidence which has a considerable influence on the accumulation of trace gases and aerosols in the troposphere (Garstang et al., 1996; Swap and Tyson, 1999).

Although atmospheric deposition is not measured at Ezamokuhle, long-term research on deposition has been conducted at Amersfoort as part of the DEBITS programme. The DEBITS data indicate that there is a general annual increase in dry deposition of both SO_2 (since 2004) and NO_2 concentrations (since 2002) in Amersfoort. Similarly there are more rain events with lower pH values from 2009 to 2014. These shifts towards higher deposition loading & more acidic rain events are ascribed to a significant increase in anthropogenic activities and population growth (Van Zyl, 2016).

In summary the results of this study has demonstrated that for Ezamokuhle air quality station: the elevated SO_2 and NO_2 levels in winter; the SO_2 18:00 peak in winter; the bi-modal particulate matter peak and the elevated particulate matter concentrations during early winter months to early spring are all attributable to residential fuel burning. Hence there is an opportunity herein to reduce human

exposure to harmful levels of air pollution by reducing emissions from residential burning. Thus supporting the roll-out of Eskom's PMV air quality offset intervention project in Ezamokuhle.

1 BACKGROUND

1.1 National Ambient Air Quality Standards (NAAQS)

An increase in both human population growth and rapid industrialisation has led to an elevation of pollutant emissions which has exacerbated both a global and a localised deterioration in air quality (Chien-Lung, 2001; Pham et al., 1995; Nunnari et al., 2004; USEPA, 1998). In turn, air pollution has often become a barrier to sustainable development in urban areas (Wang et al., 2009). Thus ambient air quality needs to be managed by the minimization & prevention of pollution sources in order to effect an improvement on the receiving environment.

Typically, for the majority of countries in the world, ambient air quality is regulated through compliance with health-based ambient air quality standards. These standards are enforced by legislation and the achievement of ambient air quality standards forms a critically important component of the air quality management planning process. The National Environment Management: Air Quality Act (Act No. 39 of 2004) (hereinafter “the AQA”) reformed the law regulating air quality in order to protect the environment. AQA is characterised by a paradigm shift from managing air pollution exclusively by the control of emissions from individual point sources, to a holistic approach based on controlling ambient concentrations in the receiving environment. Thus the effects-based approach of AQA requires the setting of ambient air quality standards (NAAQS) with the objective of protecting human health and well-being. These National Ambient Air Quality Standards (NAAQS) are shown below in Table 1.

Table 1: NAAQS (DEFF, 2009)

Pollutant	Average Period	Concentration	Frequency of Exceedance	Compliance Date
Nitrogen Dioxide (NO_2)	1 hour	106 ppb	88	Immediate
	1 year	21 ppb	0	Immediate
Ozone (O_3)	8 hour	61 ppb	11	Immediate
Inhalable particulate matter less than 2.5 µm in diameter ($PM_{2.5}$)	24 hour	40 µg/m^3	4	Immediate until 31 December 2029
	24 hour	25 µg/m^3	4	1 January 2030
	1 year	20 µg/m^3	0	Immediate until 31 December 2029
	1 year	15 µg/m^3	0	1 January 2030
Inhalable particulate matter less than 10 µm in diameter (PM_{10})	24 hour	75 µg/m^3	4	Immediate
	1 year	40 µg/m^3	0	Immediate
Sulphur Dioxide (SO_2)	10 minutes	190 ppb	526	Immediate
	1 hour	134 ppb	88	Immediate
	24 hour	48 ppb	4	Immediate
	1 year	19 ppb	0	Immediate

1.2 Activity 1: Preliminary Air Quality Assessment

Air Resource Management (Pty) Ltd (*herein referred to as* ARM) is supporting Eskom's Planning, Monitoring and Verification (PMV) Project at Ezamokuhle (Figure 1). In accordance with the scope of work, *Activity 1: Preliminary Air Quality Assessment* requires ARM to conduct an initial assessment to ascertain whether the Ezamokuhle airshed is in non-compliance with the NAAQS. ARM is utilising a phased three pronged strategy (Figure 2) of: firstly a *Status quo air quality trend analysis assessment*; secondly a *Dispersion modelling study* and finally *Ambient air quality monitoring study* in order to evaluate compliance of the NAAQS at Ezamokuhle. This focus of this report is only on the *Status quo air quality trend analysis assessment* for Ezamokuhle.

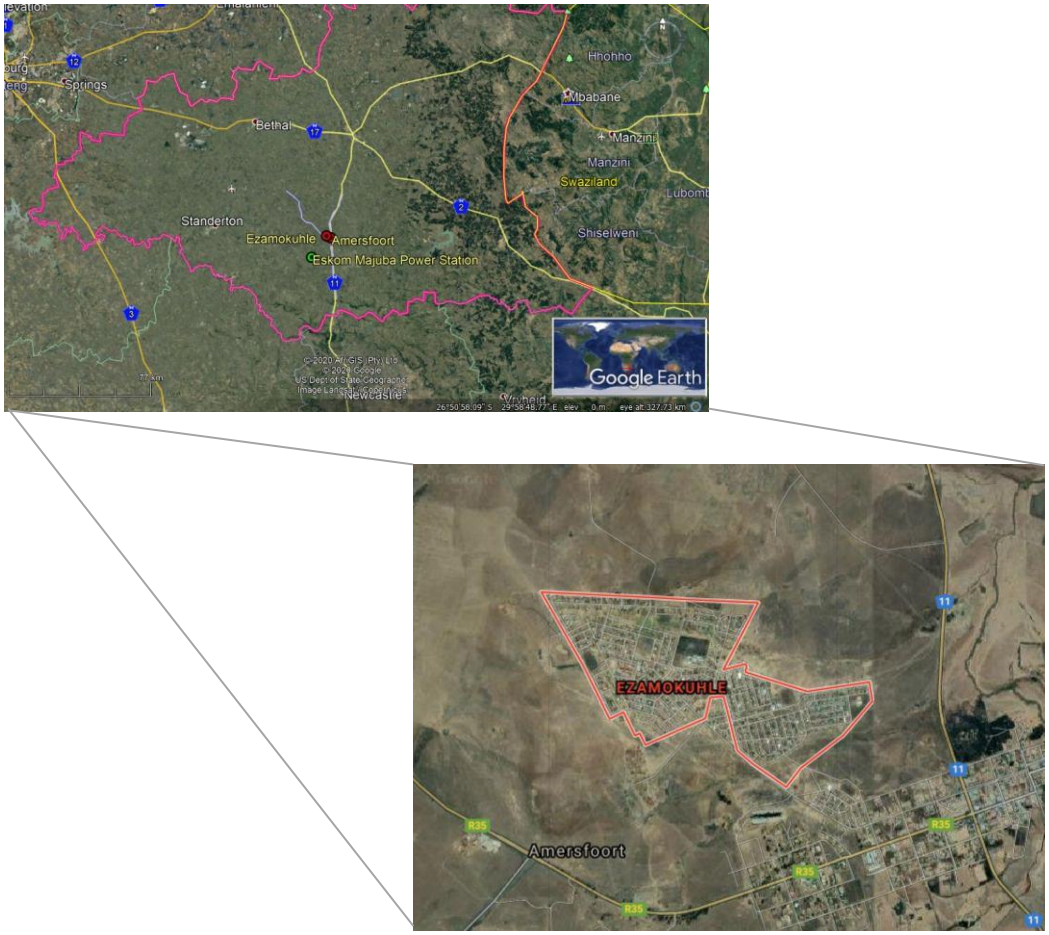

Figure 1: Locality Map for Ezamokuhle

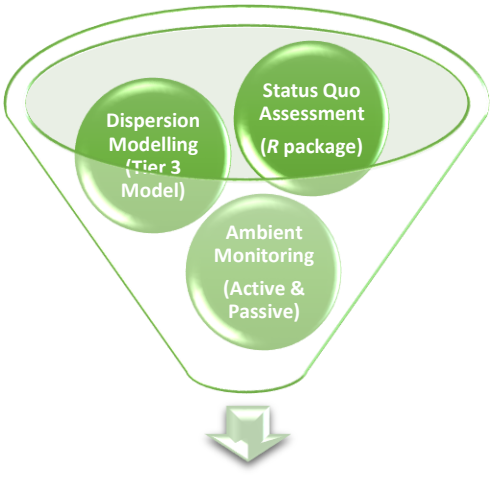

Figure 2: Strategy to evaluate NAAQS non-compliance for Ezamokuhle

2 INTRODUCTION

Worldwide an enormous and growing amount of air pollution data is collected. Typically the majority of the data are analysed in superficial ways e.g. to confirm whether an annual mean concentration is above or below a stated ambient air quality standard threshold value. Carlslaw and Ropkins (2012) demonstrated that this situation represents a considerable missed opportunity. Experience shows that considerably more information can be obtained from the analysis of data through the application of innovative data analysis techniques (Appel *et al*., 2011).

By the adoption of innovative data analysis techniques the potential benefits herein include:

i. a more comprehensive evidence base to support decision making,
ii. identification of the factors controlling pollutant concentrations (including the discovery of unexpected influences),
iii. an improvement in the quality of analyses undertaken and the enhanced validation of environmental models &
iv. potential economic benefits through better decision making and targeted actions to manage air pollution.

2.1 STUDY OBJECTIVE

The purpose of this study is to apply innovative data analysis techniques in order to help identify trends and general relations between parameters, as well as source attribution in Ezamokuhle for the period of 2018–2020. Additionally the study examined the trans-boundary movement & deposition of pollutants in the Ezamokuhle airshed.

3 METHODOLOGY

3.1 RESEARCH DESIGN

Steps taken in this study comprised of data collection, data quality control, data analysis & processing and finally an assessment of the study results.

3.1.1 DATA COLLECTION PROCESS

This study performed an analysis of trends, correlations and general relations which were based on collected measurement data (including both pollutant concentrations and meteorology) obtained from three of the air quality monitoring stations located in and around the vicinity of Ezamokuhle (Figure

3): Eskom Ezamokuhle (the *in-situ* station), Sasol Amersfoort (adjacent to Ezamokuhle), and Eskom Majuba (the industrial station).

A summary of measurement data obtained from each station is presented in Table 2. Eskom provided the measurement data (2018-2020) for the Ezamokuhle and Majuba stations whilst the data for Sasol Amersfoort station was sourced from the **Department of Environment, Forestry and Fisheries** (DEFF) *South African Air Quality Information System (SAQIS)* (http://saaqis.environment.gov.za/home/index).

Table 2: Summary of measurement data

Station	Meteorological Parameters and Pollutants provided	Start Date	End Date	Source
Ezamokuhle	Wind speed (WS), wind direction (WD), Temp (T), Rain (R) SO_2, NO_2[a] , O_3, $PM_{2.5}$	01/01/2018	31/12/2020	Eskom
Amersfoort	WS, WD, T, H_2S	01/01/2018	31/12/2020	SAQIS
Majuba	WS,WD, T, R, SO_2, NO_2 , O_3 ,PM_{10}[b, c], $PM_{2.5}$[b, c]	01/01/2018	31/12/2020	Eskom

[a] For Ezamokuhle, there were no data available for NO^2 from 17/10/20 until 11/11/20 due to a faulty analyser that was removed for repairs (*Eskom, pers comm*)

[b] For the years 2019 and 2020 there was no PM_{10} or $PM_{2.5}$ data captured. PM monitors were affected by the faulty transformer and there are no spare instrument to replace the faulty ones (*Eskom, pers comm*)

[c] There were no data available from 30/11 16:10 till 02/12 15:10 due to earth leakage trip at the site (*Eskom, pers comm*)

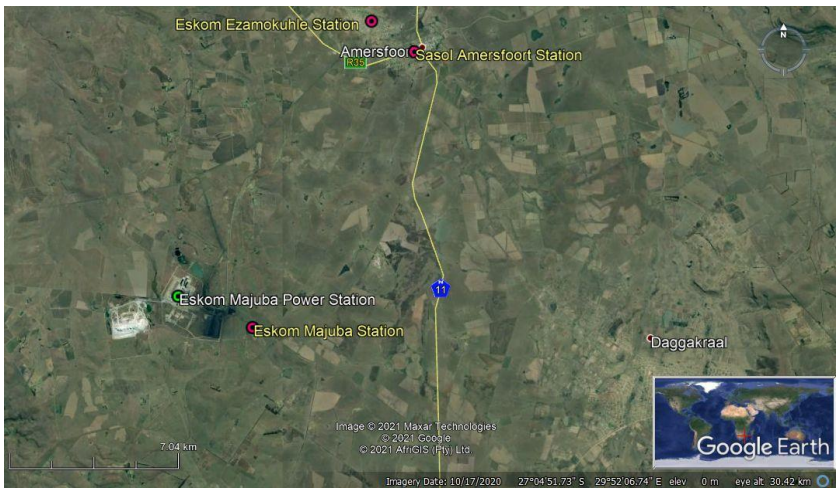

Figure 3: Location of ambient quality monitoring stations

3.1.2 Data Control Process

A quality assurance and quality control (QA/QC) process was undertaken for the measurement data obtained from each air quality station. The data was assessed in terms of the core metrics including: completeness; uniqueness; validity and consistency. Completeness evaluated the measured data in relation to the potential of it being 100% complete. Uniqueness checks were undertaken to screen for duplication of data (which may be due to error logging, equipment malfunctions etc.). A validity evaluation was undertaken to check whether the measured data conformed to the specific logging format, syntax and range, to ensure that it was usable. A consistency check was done to test for the absence of a difference, when two or more pollutants with similar traits were compared (for example PM_{10} and $PM_{2.5}$).

According to the DEFF guidance (DEFF, 2016), a minimum data capture recovery rate of 80% must be achieved for a station (Table 3). The statistical summary of all data used in this study is presented in Table 4 to 6 & Figures 4 to 7. It's evident (Table 4) that the monitoring station at Ezamokuhle recorded good quality data, with an average data availability of 96% in contrast Amersfoort (Table 5) which was very poor with an average data availability of only 16%. For Majuba station (Table 6), the average data availability is 69%. However it must be also noted herein that no PM_{10} or $PM_{2.5}$ data was captured for the period 2019 to 2020 due to non-operational PM analysers for Majuba hence impacting on the station's overall data capture recovery rate.

Table 3: DEFF Guidance: Station Data Recovery (DEFF, 2016)

Parameter Time Resolution	Required Proportion of Valid Data
1 hour values	80 % of values (i.e. 48 minutes)
8 hours values	75 % of values (i.e. 6 hours)
24 hour average value	83% of values (i.e. 20 hours)
Annual mean	80 % of the 1 hour values over winter (April to September)*
Number of exceedances per year	Five out of six months over the winter season (April to September)*

*** In cases where the percentages are not reached, the annual averages and exceedances must be noted.**

Table 4: Statistical Summary of 10 minute average pollutant concentrations and meteorological parameters for the Eskom Ezamokuhle monitoring station

Variable	Unit	N	% valid	% missing	n (missing)	Median	Mean	Max
WS	m/s	158500	**97.2**	2.8	4438	2.7	2.9	15.1
WD	Deg	164714	**97.2**	2.8	4612	174.4	183.4	360
Temp	Deg	156923	**97.4**	2.6	4080	15.4	15.4	37
SO_2	Ppb	157047	**95.7**	4.3	6753	3.8	6.9	288.3
NO_2	Ppb	157686	**93**	7	11038	4.2	6	140.3
O_3	Ppb	159537	**95.9**	4.1	6541	31.2	33.9	153.2
$PM_{2.5}$	ug/m3	158254	**92.9**	7.1	11236	5.5	13.3	548.5

Table 5: Statistical summary of hourly average pollutant concentrations and meteorological parameters for the Sasol Amersfoort monitoring station

Variable	Unit	N	% valid	% missing	n (missing)	Median	Mean	Max
WS	m/s	35523	**16**	84	29840	1.5	1.9	10.3
WD	Deg	23620	**16**	84	19841	142.3	163	359.8
Temp	Deg	35522	**16**	84	29839	14.5	14	33.2
H_2S	Ppb	35525	**16**	84	29841	1.8	2.8	251.4

Table 6: Statistical summary of 10 minute average pollutant concentrations and meteorological parameters for Eskom Majuba monitoring station

Variable	Unit	N	% valid	% missing	n (missing)	Median	Mean	Max
WS	m/s	156978	**90.9**	9.1	14285	3.9	4.1	17.2
WD	Deg	157969	**80.6**	19.4	30646	152.1	179.9	360
Temp	Deg	156759	**94.2**	5.8	9092	14.7	15	36.2
SO_2	Ppb	157568	**69.2**	30.8	48531	4.3	9	807.3
NO_2	Ppb	157733	**80.9**	19.1	30127	3	4.8	110.5
O_3	Ppb	158106	**83**	17	26878	32.7	34.5	125.1
PM_{10}	ug/m3	157759	**27.3**	72.7	114691	20.2	27.9	519.8
$PM_{2.5}$	ug/m3	157778	**25.8**	74.2	117071	11.6	15.1	401.8

Figures 4 to 6 illustrate the key graphical and statistical summaries for the collected ambient air quality data. The plots in the left panel show the time series data, where blue shading shows the presence of data and yellow missing data. The daily mean values are also shown in dark blue line scaled to cover the range in the data from zero to the maximum daily value. As such, the 10 minutes values are indicative of an overall trend rather than conveying quantitative information. For each pollutant, the overall summary statistics are given. For each year (2018 to 2020) the percentage data capture is shown in green font. The panels on the right show the distribution of each species using a histogram plot.

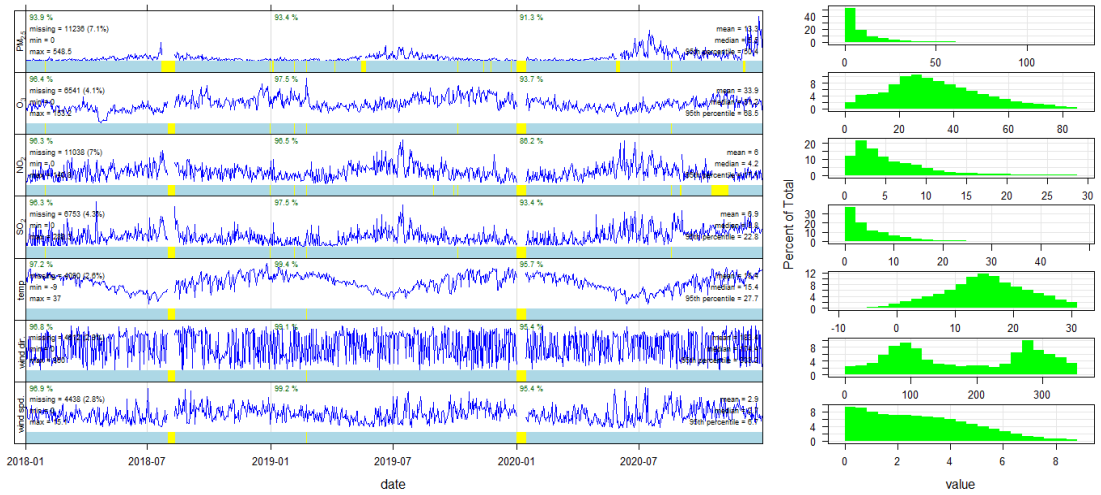

Figure 4: Key graphical and statistical summaries for the Eskom Ezamokuhle monitoring station

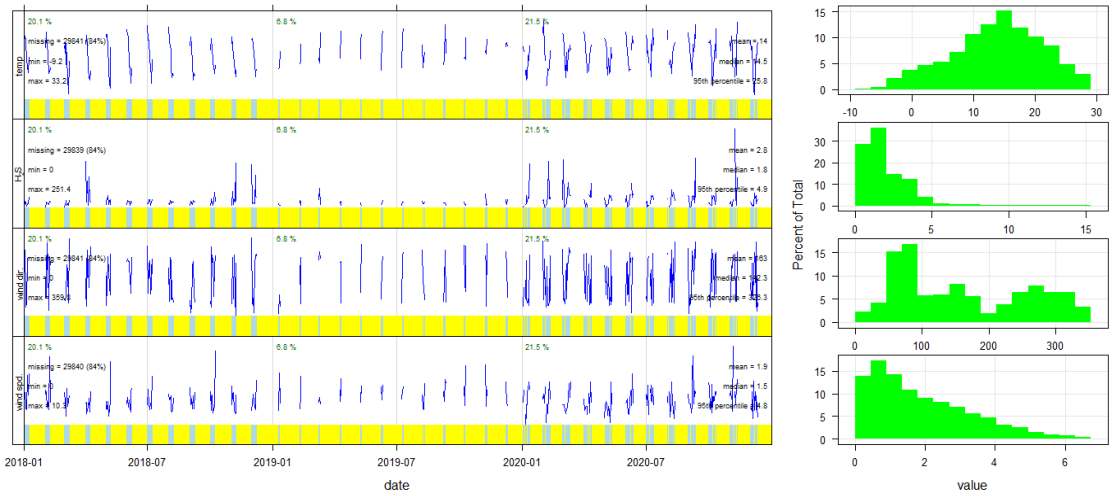

Figure 5: Key graphical and statistical summaries for the Sasol Amersfoort monitoring station

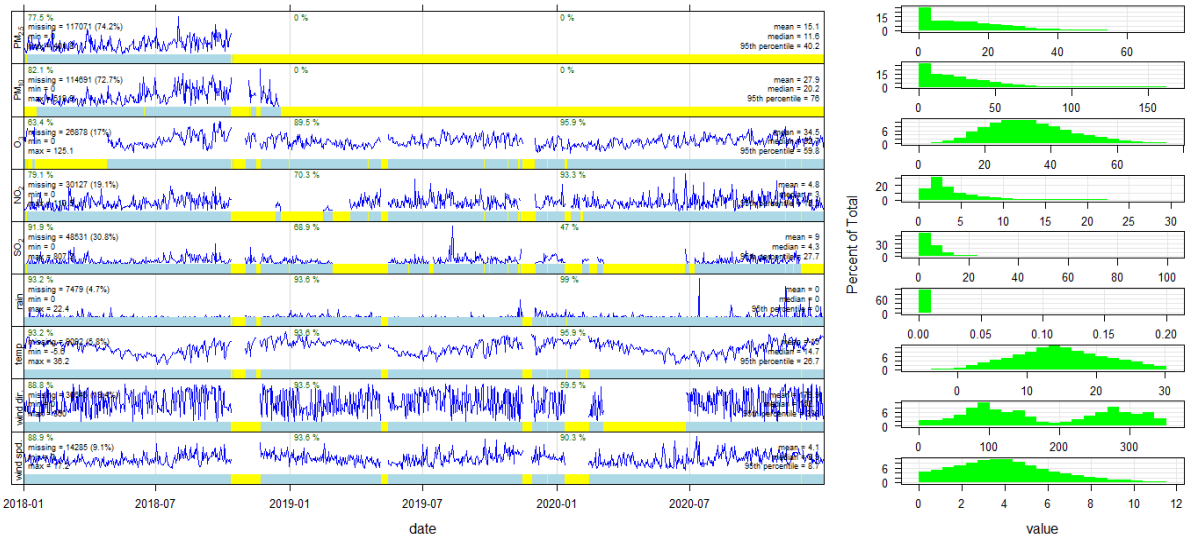

Figure 6: Key graphical and statistical summaries for the Eskom Majuba monitoring station

3.1.3 Data Analysis & Processing

Openair is an air quality model for statistically analysing semi-empirical mathematical relationships between air pollutant concentration and other factors that may affect it (Tiwary, 2010). The Openair model can analyze emissions of pollutant sources, pollutant characteristics, trend estimates and model evaluations. Additionally Openair model has the advantage of data manipulation or interpolation, statistical data analysis, creation and visualization of high-quality graphics (Carslaw, 2015).

The Openair model has been successfully applied to determine the potential emission sources based on urban air quality measurements (Munir *et al*., 2016, Czernecki *et al*., 2016) as well as for air quality research campaigns (Crilley *et al*. 2017), studies concerning pollution exposure (Pattinson *et al*. 2016), and natural events (Salvador *et al*. 2014; Schweizer, Cisneros 2014). Often multiple functions provided in Openair are combined to provide comprehensive information & insight for the analyzed data (Crilley *et al*., 2015 and Jang *et al*., 2016).

The relationship and trends of concentrations, including PM_{10}, $PM_{2.5}$, SO_2, NO_2, O_3, H_2S and meteorological parameters such as wind speed and direction, temperature for the three air quality monitoring stations (Table 2) were examined using the Openair model.

4 RESULTS & DISCUSSION

4.1 TREND ANALYSIS AND RELATIONSHIPS

4.1.1 TIME VARIATION & TREND LEVEL PLOTS

For air quality, the variation of a pollutant by time of day and day of week can reveal useful information concerning the likely sources. Time series (mean with 95% confidence interval) of ambient pollutant concentrations measured at the: Eskom Ezamokuhle (Figure 7); Eskom Majuba (Figure 8) and the Sasol Amersfoort (Figure 9) station show the variation of these pollutants over daily, weekly and annual cycles. Additionally the trend level plots (Figures 12 to 21) show the variation in pollutant concentrations by year and hour of the day for these respective air quality stations.

NITROGEN DIOXIDE (NO_2)

The Ezamokuhle NO_2 results (Figure 7) explicitly reveal that the variability of this pollutant concentration is conditioned by vehicle emissions. Daily and weekly variation corresponds to the cyclical nature of traffic volume with marked peaks in concentration on weekdays around the early-morning and late-afternoon rush-hours. Figure 7 shows NO_2 concentrations plotted by time-of-day for Ezamokuhle. It shows a clear rise in concentrations with the peak of the morning rush-hour at around 06:00 and a second less marked rise with the evening rush-hour peaking at around 18:00.

For the Eskom Majuba station, there is an increased NO_2 concentrations at just before midday due to the break-up of an elevated inversion layer, in addition to the development of daytime convective conditions causing the plume to be brought down to ground level relatively close to the point of release from tall stacks.

The winter (Figure 7 & 8) elevation of NO_2 shows the contribution of residential fuel burning to the ambient NO_2 concentrations at the Eskom Ezamokuhle and Majuba stations. Additionally the trend level plots (Figure 12 and 13) indicate the residential fuel burning for winter occurs generally for the period between 17:00 to 22:00 with emissions peaking at 18:00. Figure 8 indicates that for the period 2018 to 2020, that the months of: March; August and November recorded the highest NO_2 concentrations for the Eskom Majuba station. A comparison of the trend level NO_2 plot (Figure 13) shows that the peaks for these months occurred at 12:00 thus indicating the impact of tall stack emission source.

SULPHUR DIOXIDE (SO_2)

For both the Eskom Ezamokuhle and Majuba stations, SO_2 (Figure 7 and 8) show a typically industrial signature with increased SO_2 concentrations as just before midday due to the break-up of an elevated inversion layer, in addition to the development of daytime convective conditions causing the plume to be brought down to ground level relatively close to the point of release from tall stacks.

The winter (June, July and August) elevation of SO_2 shows the contribution of residential fuel burning to the ambient SO_2 concentrations at the Eskom Ezamokuhle and Majuba stations. It's evident for the Eskom Ezamokuhle station (Figure 7), there is a second less pronounced peak compared to midday that occurs consistently throughout the entire week at 18:00. A comparison of the trend level plot for Ezamokuhle (Figure 14) clearly indicates that the 18:00 peak occurs in winter (peaking in the months of June and July) thus indicating the impact of residential fuel burning emissions.

Figure 8 indicates that for the period 2018 to 2020, that the months of: March; August and November recorded the highest SO_2 concentrations for the Eskom Majuba station. A comparison of the trend level SO_2 plot (Figure 15) shows that the peaks for these months occurred at 12:00 thus indicating the impact of a tall stack emission source/s.

OZONE (O_3)

O_3 in the lower troposphere forms through the reaction between oxides of nitrogen and volatile organic compounds in the presence of the ultraviolet portion of sunlight (<420nm) (Tienhoven et al., 2005). For both the Eskom Ezamokuhle and Majuba stations, O_3 (Figure 7 and 8) show a strong diurnal & seasonal variation. The surface ozone concentrations increase from a minimum near sunrise to a maximum in the afternoon (around 15:00), then decrease again to the early morning minimum throughout the entire week (Figure 16 & 17). The highest concentrations occur around September (Figure 16 & 17), which coincides with the biomass burning season in Southern Africa. Biomass burning is seasonal and occurs almost exclusively during the winter and into spring, from July to September (Silva et al., 2002).

HYDROGEN SULPHIDE (H_2S)

At the Sasol Amersfoort station, there is an increased H_2S concentrations at just before midday (Figure 9) due to the break-up of an elevated inversion layer, in addition to the development of daytime convective conditions causing the plume to be brought down to ground level relatively close to the point of release from tall stacks. This unimodal peak signal is present throughout the week

with monthly peaks occurring in the months of April and November (Figure 18). It's plausible that these peak monthly H_2S concentrations are linked to the process operating conditions from the tall stack emission source for these respective months.

PARTICULATE MATTER (PM_{10} & $PM_{2.5}$)

The bi-modal particulate matter peak for both the Eskom Ezamokuhle and Majuba stations (Figure 10 and 11) is a typical profile for residential fuel burning. A morning peak occurs at 07:00 whilst the evening peak occurs at 18:00. The morning peaks reduces towards midday as the inversion layer rises & improves the mixing height of the planetary boundary layer.

Monthly variation of particulate matter shows elevated concentrations during early winter months to early spring (May to September) due to the greater contribution from domestic fuel burning, dust from uncovered soil and the lack of the settling influence of rainfall. It's noted that a monthly peak is measured for the Eskom Ezamokuhle station for the month of December (Figure 10). A comparison of the trend level plot for the Eskom Ezamokuhle station (Figure 19) shows that for the years 2020, these emissions occur between 17:00 to 21:00 with emissions peaking at 18:00 thus indicating the impact of a residential fuel burning source (perhaps cooking).

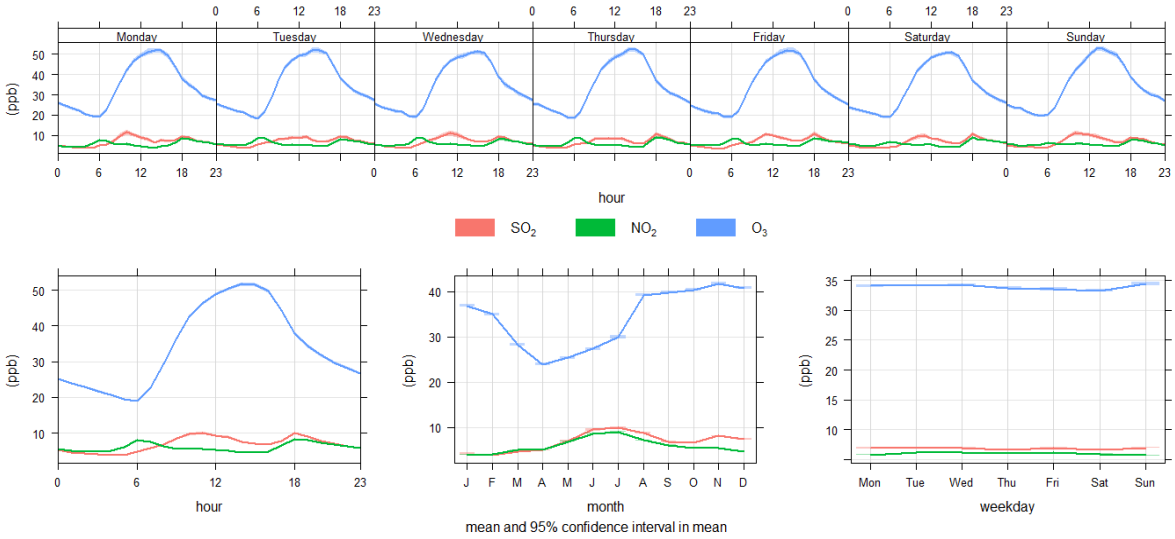

Figure 7: Mean pollutant concentrations in ppb for the Eskom Ezamokuhle air quality station calculated for hourly mean during weekdays and a single day, monthly, and daily mean (2018–2020).

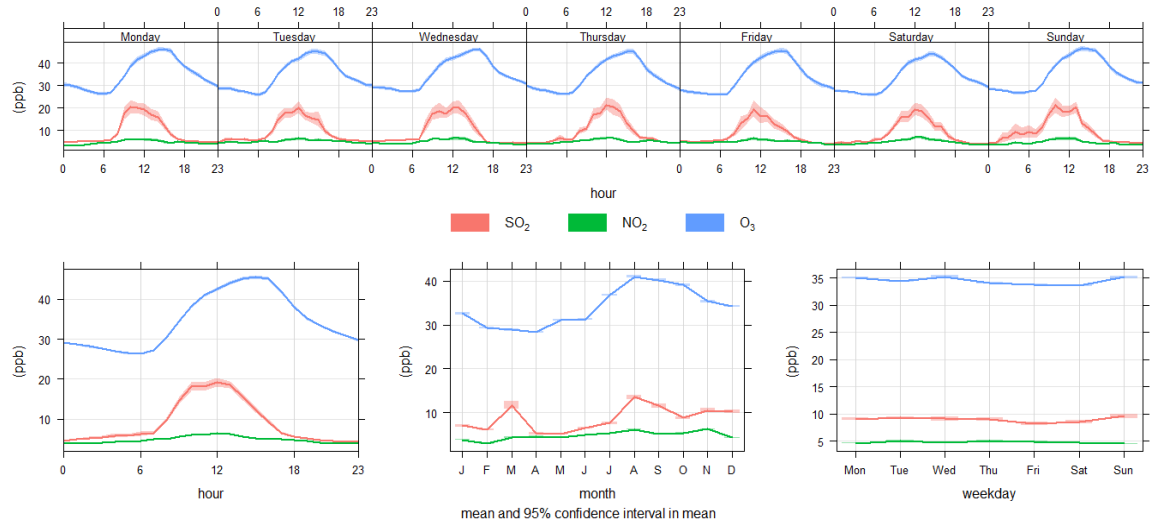

Figure 8: Mean pollutant concentrations in ppb for the Eskom Majuba air quality station calculated for hourly mean during weekdays and a single day, monthly, and daily mean (2018–2020).

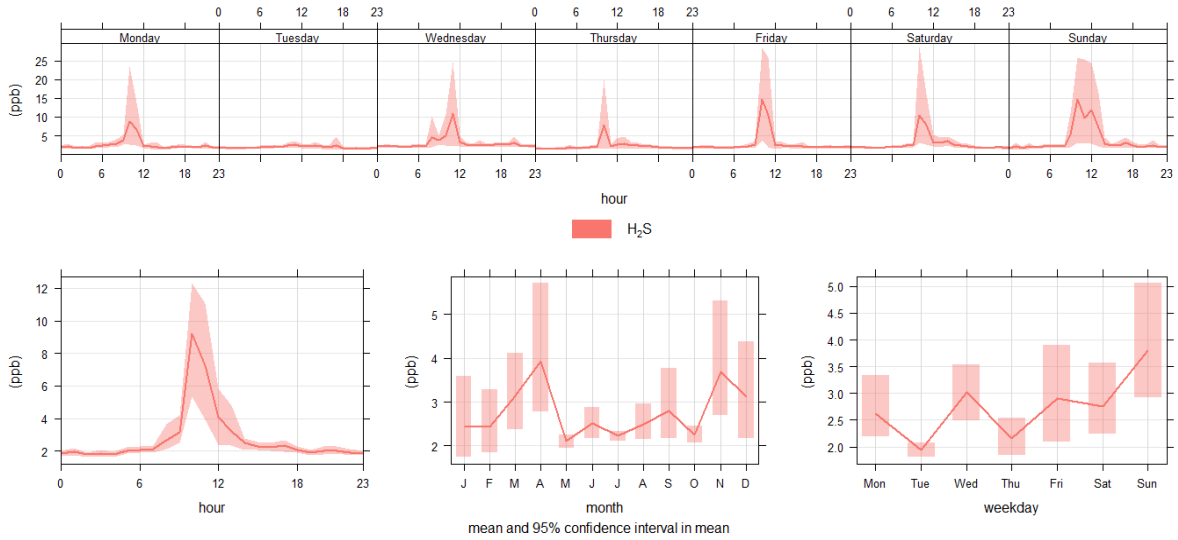

Figure 9: Mean pollutant concentration in ppb for the Sasol Amersfoort air quality station calculated for hourly mean during weekdays and a single day, monthly, and daily mean (2018–2020).

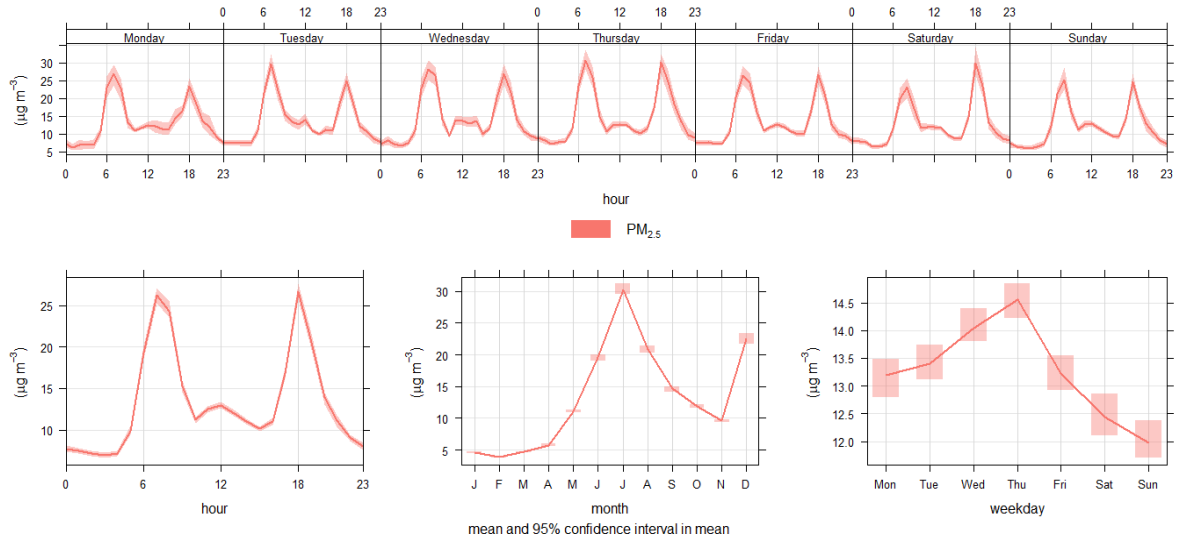

Figure 10: Mean pollutant concentrations in ug/m3 for the Eskom Ezamokuhle air quality station calculated for hourly mean during weekdays and a single day, monthly, and daily mean (2018–2020).

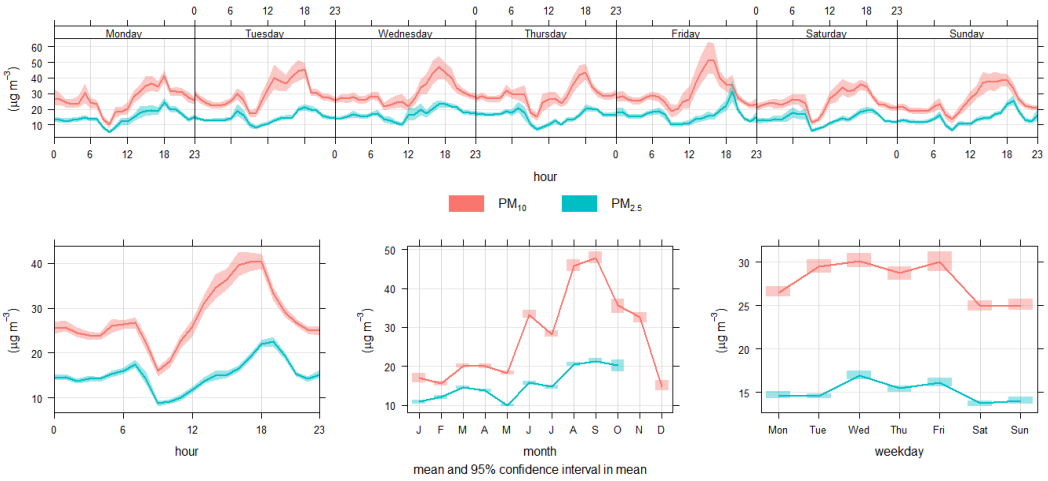

Figure 11: Mean pollutant concentrations in ug/m^3 for the Eskom Majuba air quality station calculated for hourly mean during weekdays and a single day, monthly, and daily mean (Only 2018).

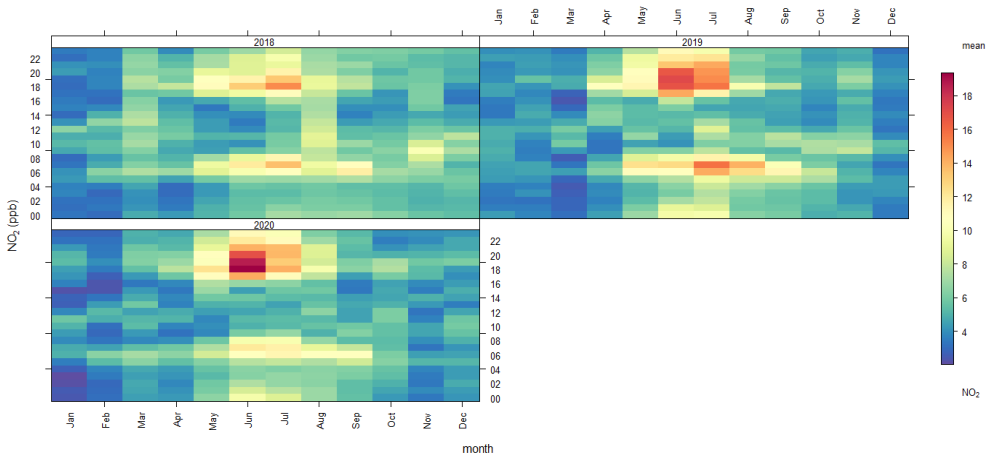

Figure 12: Trend level plot for NO_2 measured at the Eskom Ezamokuhle Monitoring Station

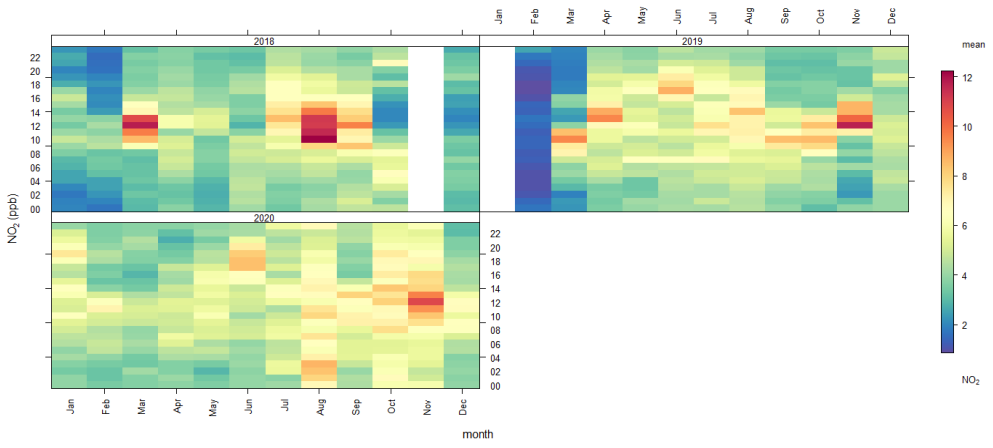

Figure 13: Trend level plot for NO_2 measured at the Eskom Majuba Monitoring Station

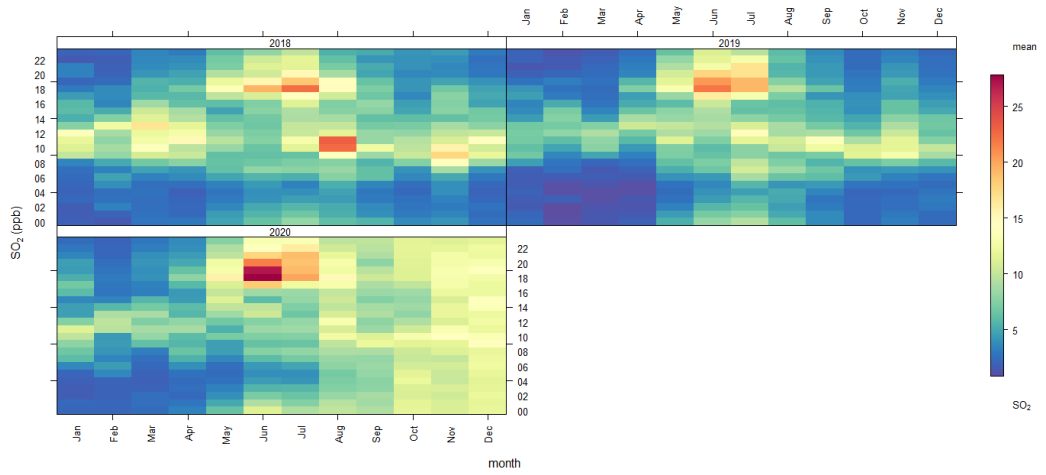

Figure 14: Trend level plot for SO_2 measured at the Eskom Ezamokuhle Monitoring Station

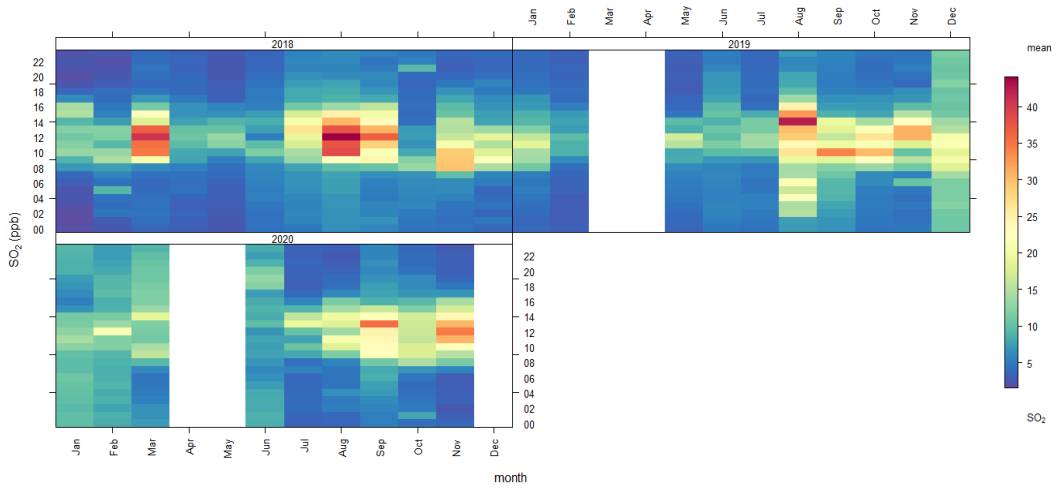

Figure 15: Trend level plot for SO_2 measured at the Eskom Majuba Monitoring Station

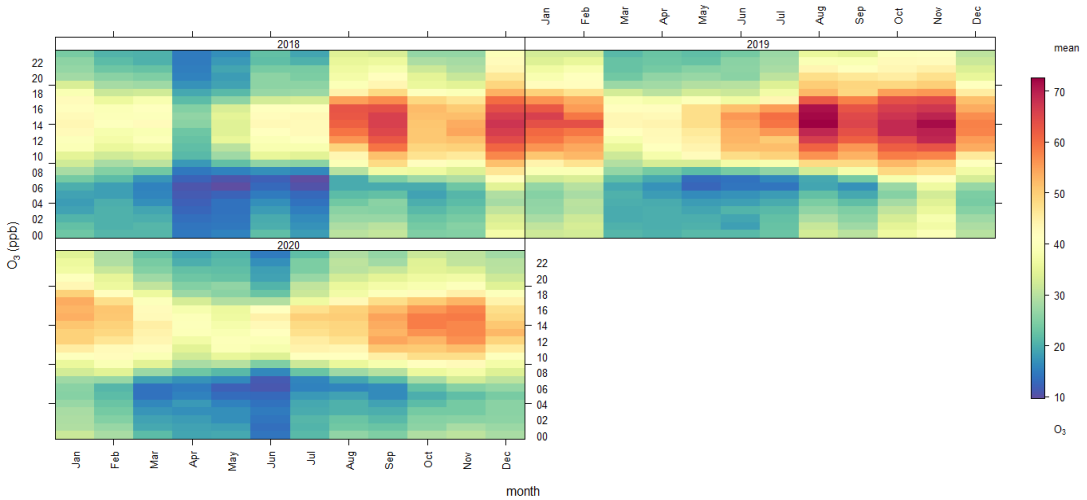

Figure 16: Trend level plot for O_3 measured at the Eskom Ezamokuhle Monitoring Station

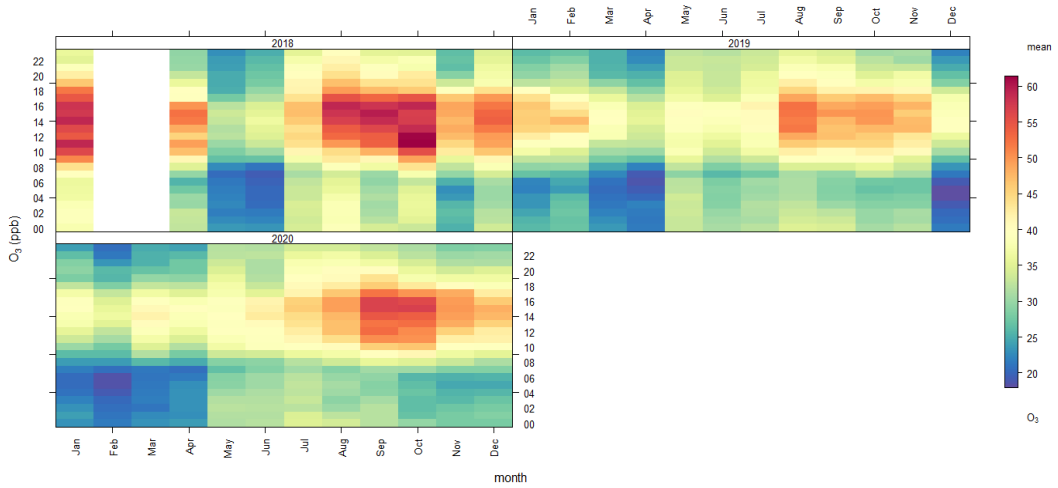

Figure 17: Trend level plot for O_3 measured at the Eskom Majuba Monitoring Station

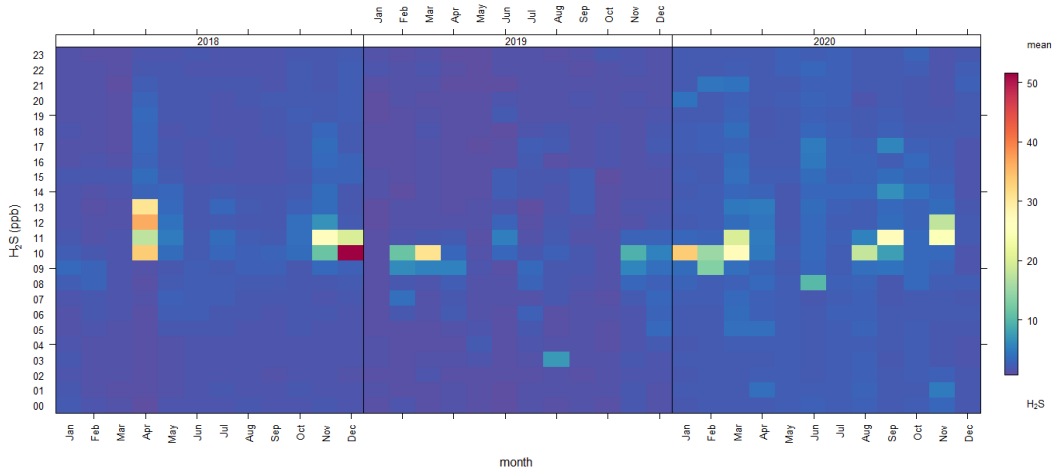

Figure 18: Trend level plot for H_2S measured at the Sasol Amersfoort Monitoring Station

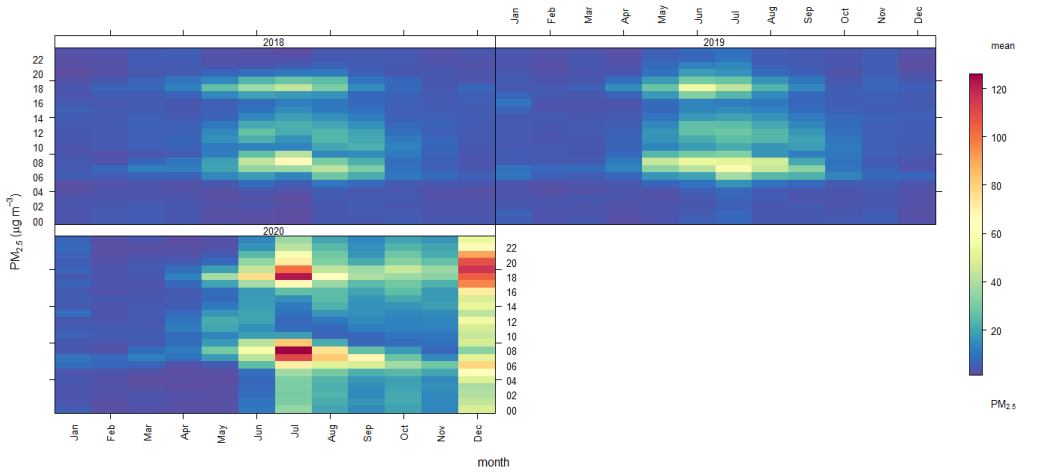

Figure 19: Trend level plot for $PM_{2.5}$ measured at the Eskom Ezamokuhle Monitoring Station

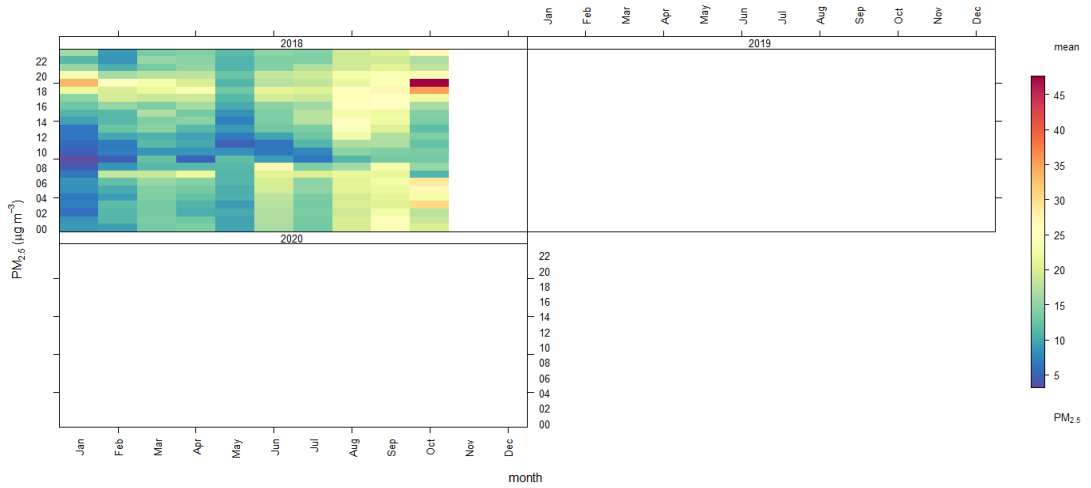

Figure 20: Trend level plot for $PM_{2.5}$ measured at the Eskom Majuba Monitoring Station

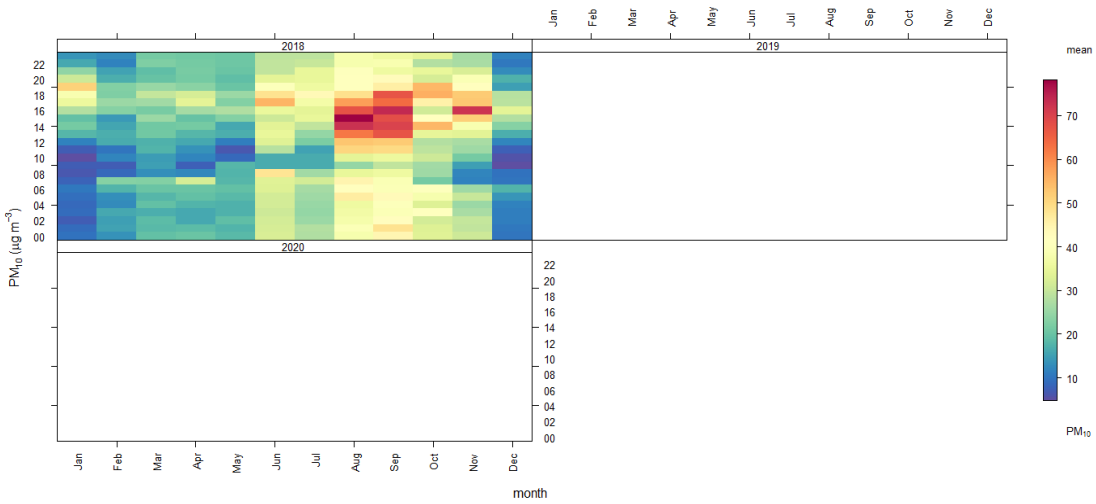

Figure 21: Trend level plot for PM_{10} measured at the Eskom Majuba Monitoring Station

4.1.2 Wind Direction, Speed & Concentration

Air quality is strongly influenced by meteorology. Meteorological mechanisms govern the dispersion, transformation, and eventual removal of pollutants from the atmosphere (Seaman, 2000). The analysis of hourly average meteorological data is necessary to facilitate a comprehensive understanding of the dispersion potential of the site. The horizontal dispersion of pollution is largely a function of the wind field. The wind speed determines both the distance of downward transport and

the rate of dilution of pollutants. The wind rose is a very useful way for showing how wind speed and wind direction conditions vary by year.

4.1.2.1 WIND DIRECTION

The 16 spokes of a wind rose represent the directions from which winds blew for a specific period. The dotted circles in the wind rose provide information regarding the frequency of occurrence of wind speed and direction categories whilst the colours used in the wind roses reflect the different categories of wind speeds. The period wind field for the three ambient air quality monitoring stations (Table 2) for the period 2018 to 2020 in Figure 12 to 17.

For the Eskom Ezamokuhle air quality station the average wind speed for the period 2018 to 2020 (Figure 22) was recorded at 2.93 meters/second with calm condition 0.1%. Calm condition means that wind speed is recorded at zero meter/second (Carlaw, 2015). The predominant wind directions were both easterly and westerly (~ 15% frequency of occurrence) followed by north-west wind (~ 12% frequency of occurrence) with maximum wind speed of 6 – 15 meters/second.

The wind speed and direction data also demonstrate a seasonal signal Eskom Ezamokuhle air quality station (Figure 23). For the spring and summer months, the average wind speed for was recorded between ~ 3 to 3.4 meters/second with the predominant wind direction been an easterly wind (~ 15% to 20% frequency of occurrence for the period) followed by both a westerly wind and a north-westerly wind (~ 10% frequency of occurrence). Whilst for the autumn and winter winds, the average wind speed for was recorded between ~ 2.4 to 2.8 meters/second with the predominant wind direction been a westerly wind (~ 15% to 25% frequency of occurrence for the period) followed by a north-westerly wind (~ 10% to 15% frequency of occurrence for the period).

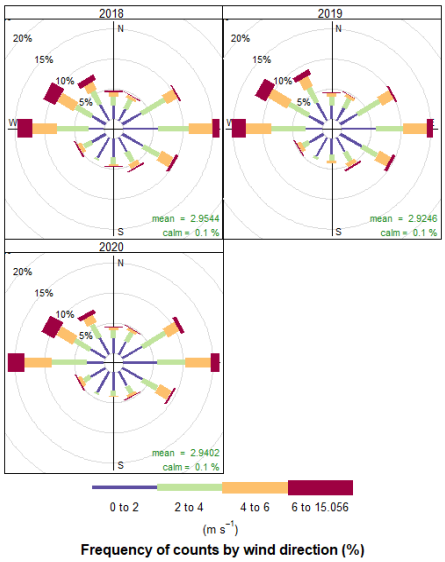

Figure 22: Annual wind rose for the Eskom Ezamokuhle station for the period 2018 to 2020

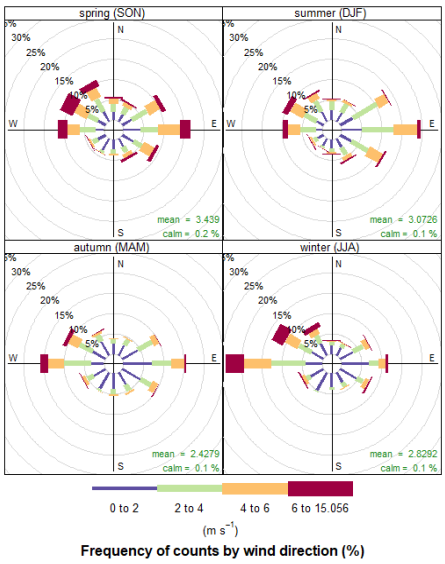

Figure 23: Seasonal wind rose for the Eskom Ezamokuhle station for the period 2018 to 2020

For the Eskom Majuba air quality station the average wind speed for the period 2018 to 2020 (Figure 24) was recorded at 4.1 meters/second with calm condition: 0.1% (2018); 0.2 % (2019) and 34.1% (2020). Calm condition means that wind speed is recorded at zero meter/second (Carlaw, 2015). The predominant wind direction is easterly (~ 20% to 10% frequency of occurrence for the period) followed by a westerly wind (~ 14% to 9% frequency of occurrence for the period) with maximum wind speed of 6 – 17 meters/second.

The wind speed and direction data also demonstrate a seasonal signal Eskom Majuba air quality station (Figure 25). For spring the average wind speed for was recorded ~4.8 meters/second with the predominant wind direction been an easterly wind (~ 16 frequency of occurrence) followed by both a westerly wind and north-westerly wind (~ 10% frequency of occurrence). The summer and autumn average wind speed recorded was between ~3.4 to 4.3 meters/second with the predominant wind direction been an easterly wind followed by a westerly wind. However it's noted that a significant percentage of calm conditions were recorded for autumn (33 %). The average wind speed for was recorded for winter was ~4.1 meters/second with the predominant wind direction been a westerly wind (~ 16 frequency of occurrence) followed by both a north-westerly wind (~ 10% frequency of occurrence). Calm conditions recorded for winter were 9.4%.

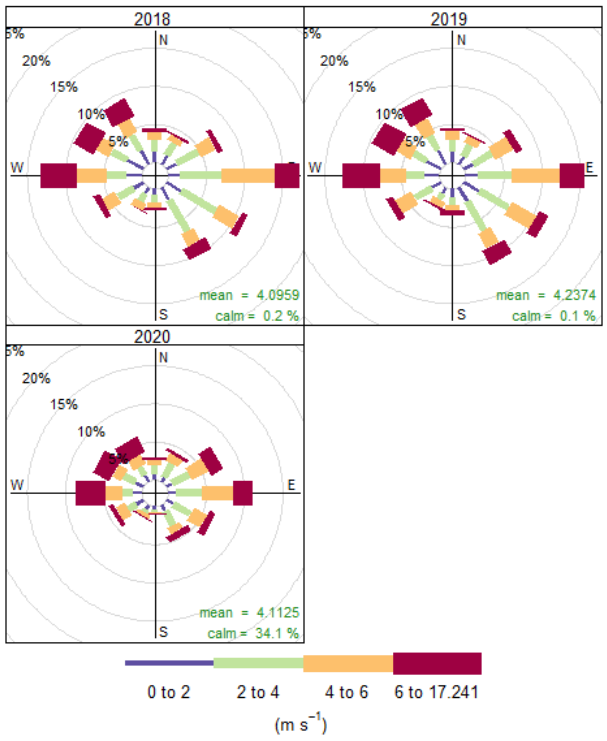

Figure 24: Annual wind rose for the Eskom Majuba station for the period 2018 to 2020

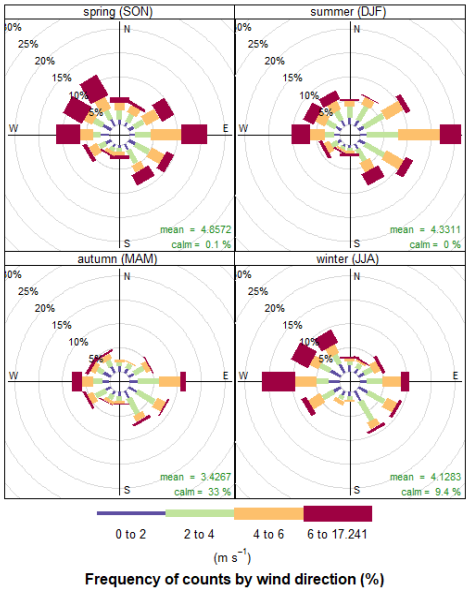

Figure 25: Seasonal wind rose for the Eskom Majuba station for the period 2018 to 2020

Sasol Amersfoort air quality station average wind speed for the period 2018 to 2020 (Figure 26) was recorded between 1.8 to 2.3 meters/second. The calm conditions of 3.4% (2018); 3.7 % (2019) and 8.4% (2020) were recorded. The predominant wind direction is north easterly (~ 18% frequency of occurrence) followed by a westerly wind (~ 10% frequency of occurrence for the period) with maximum wind speed of 6 – 10 meters/second.

The wind speed and direction data also demonstrate a seasonal signal for the Sasol Amersfoort air quality station (Figure 27). For the spring and summer months, the average wind speed for was recorded is ~ 2 meters/second with the predominant wind direction been a north-easterly wind (~ 20% frequency of occurrence) followed by a westerly wind (~ 10% frequency of occurrence). Whilst for the autumn and winter winds, the average wind speed for was recorded ~ 1.8 meters/second with the predominant wind direction been a north easterly wind (~ 16% frequency of occurrence) followed by a south-easterly wind (~ 11% frequency of occurrence).

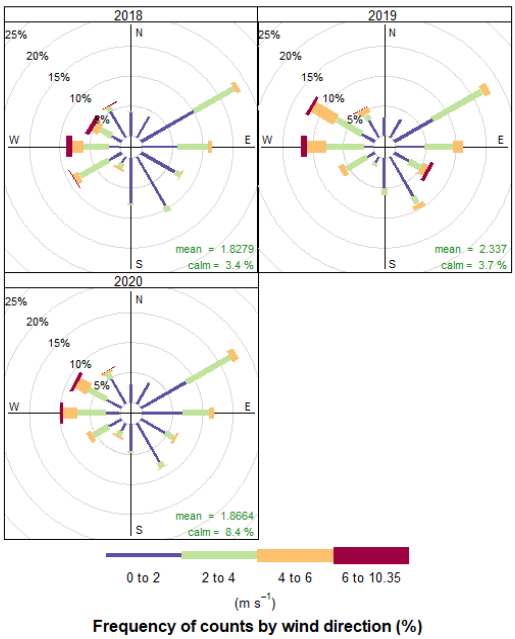

Figure 26: Annual wind rose for the Sasol Amersfoort station for the period 2018 to 2020

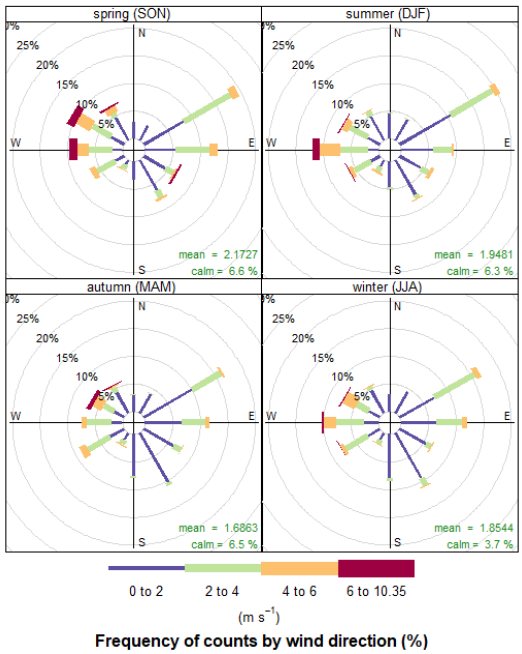

Figure 27: Seasonal wind rose for the Sasol Amersfoort station for the period 2018 to 2020

4.1.2.2 WIND SPEED

Wind drives the atmospheric transport and strongly affects vertical air mixing and thus the ventilation of the urban air (Grundstrom et al., 2015). The understanding of how wind speed affects ground–level air pollution concentrations is relatively well established.

Stagnant atmospheric conditions with calm, clear weather often lead to stable atmospheric stratification which can transform into strong nocturnal temperature inversions due to rapid surface cooling. The resulting restriction in vertical air mixing near the surface consequently leads to poor air quality (Delaney and Dowding, 1998; Janhall et al., 2006; Olofson et al., 2009). Low wind speeds deteriorate air quality with respect to pollutants emitted near the ground due to restricted air ventilation (Jones et al., 2010). In contrast higher wind speeds are associated with increased dispersion and mixing of atmospheric pollutants which may result in low ambient pollution concentrations.

MONTHLY WIND SPEED AVERAGES

Figures 28 to 30 illustrates the monthly wind speed average for the Eskom Ezamokuhle and Majuba stations as well as the Sasol Amersfoort station. For the Eskom Ezamokuhle and Majuba stations the period January until May the wind speed pattern shows a decrease from with low averages recorded until July. This is associated with less mixing and dispersion of pollutants thus resulting in elevated ambient concentrations in winter (Liebenberg, 1999).

Conversely, there is an increase in wind speeds recorded from August until November. This is associated with increased dispersion and mixing of atmospheric pollutants which may result in lower ambient pollution concentrations. It's noted that however for all three stations, December shows a lower average wind speed in comparison to the period August until November. Additionally it's also interesting to note that annual windrose for the Eskom Majuba station indicates that a high percentage of calm conditions (34.1%) were experienced in 2020. This can lead to stable atmospheric stratification which can transform into strong nocturnal temperature inversions due to rapid surface cooling. The resulting restriction in vertical air mixing near the surface consequently leads to poor air quality.

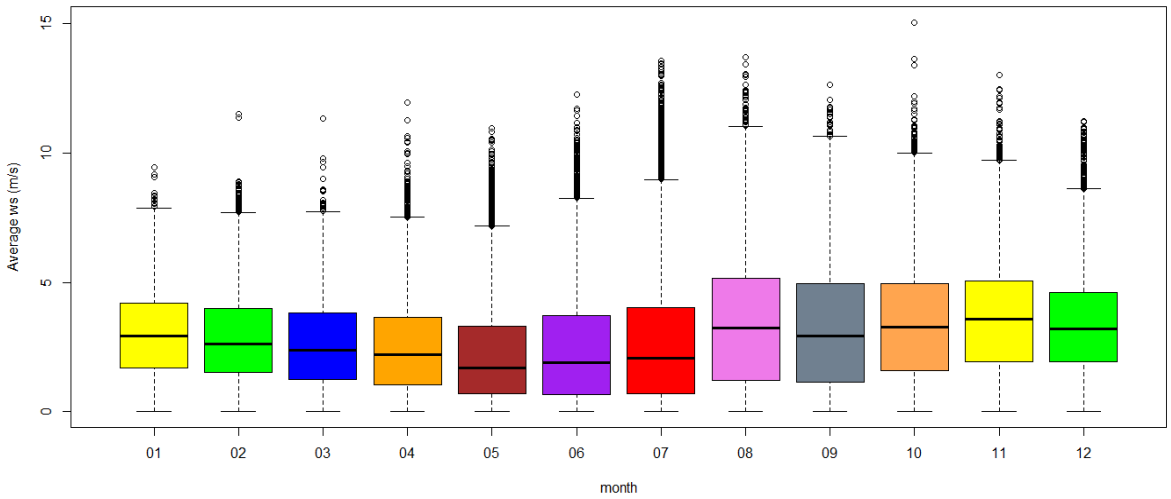

Figure 28: Monthly wind speed averages for the Eskom Ezamokuhle Station (whisker & box indicates interquartile range, diamond indicate outliers and the bars indicate the min and max value)

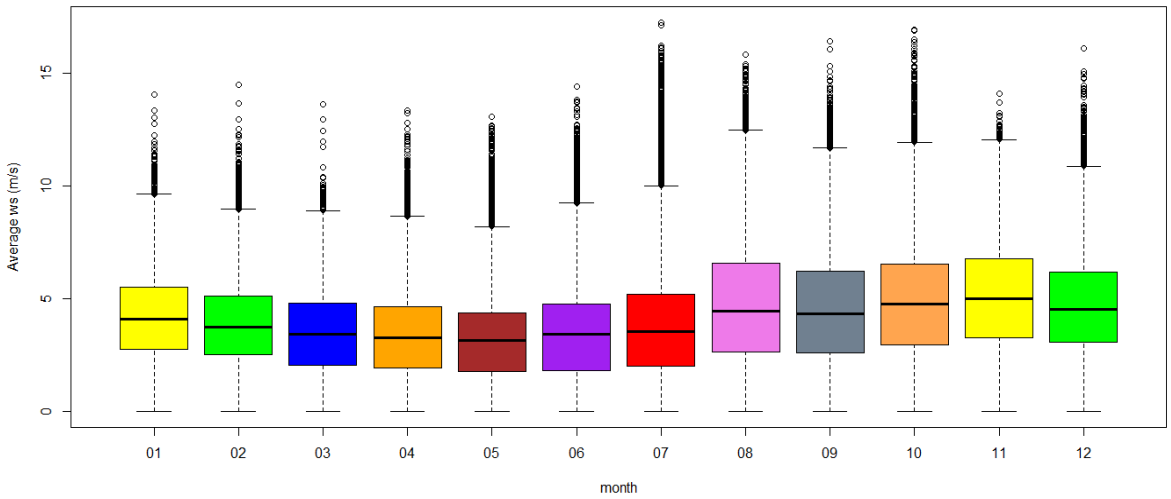

Figure 29: Monthly wind speed averages for the Eskom Majuba Station (whisker & box indicates interquartile range, diamond indicate outliers and the bars indicate the min and max value)

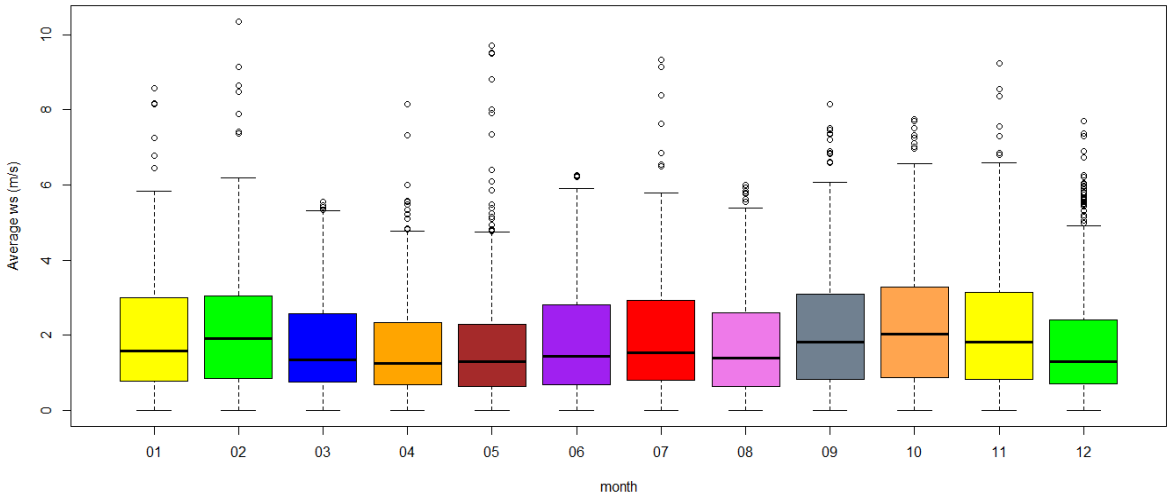

Figure 30: Monthly wind speed averages for the Sasol Amersfoort Station (whisker & box indicates interquartile range, diamond indicate outliers and the bars indicate the min and max value)

DIURNAL WIND SPEED AVERAGES

Figures 31 to 33 illustrate the diurnal wind speed average for the Eskom Ezamokuhle and Majuba stations as well as the Sasol Amersfoort station. For all stations, lower wind speeds are logged from 18h00 until 07h00. This is associated with elevated atmospheric pollution concentrations due to less mixing and dispersion. The wind speeds then increase from 08h00 until 17h00. This is associated with less pollution concentrations influenced by an increase in the mixing and dispersion of atmospheric pollutants (Liebenberg, 1999).

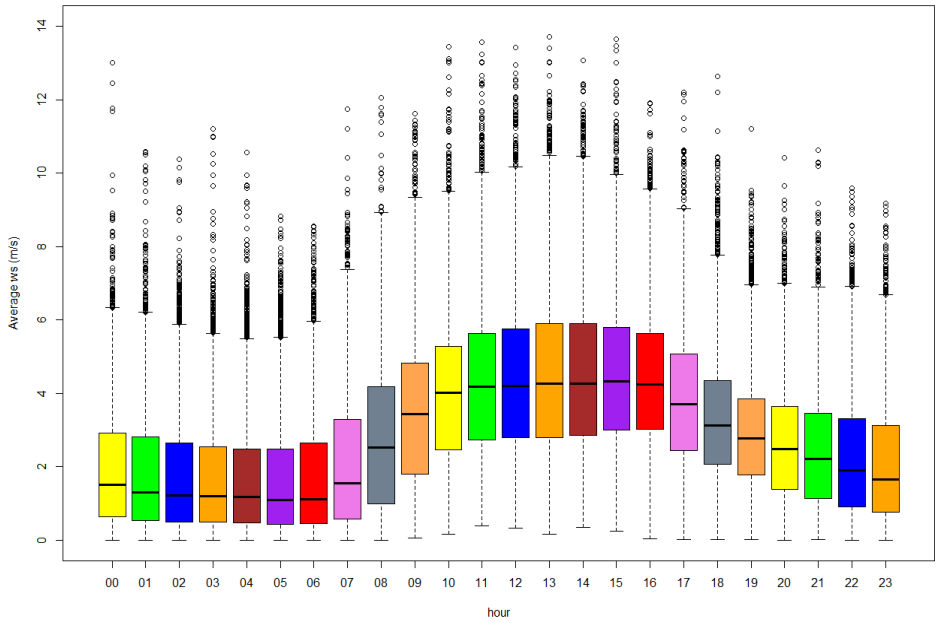

Figure 31: Diurnal wind speed averages for the Eskom Ezamokuhle Station (whisker & box indicates interquartile range, diamond indicate outliers and the bars indicate the min and max value)

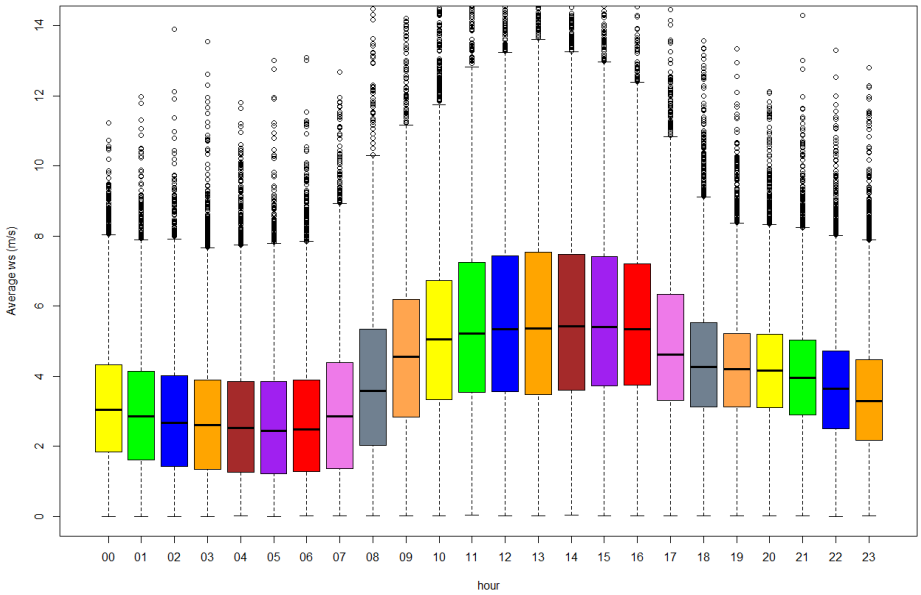

Figure 32: Diurnal wind speed averages for the Eskom Majuba Station (whisker & box indicates interquartile range, diamond indicate outliers and the bars indicate the min and max value)

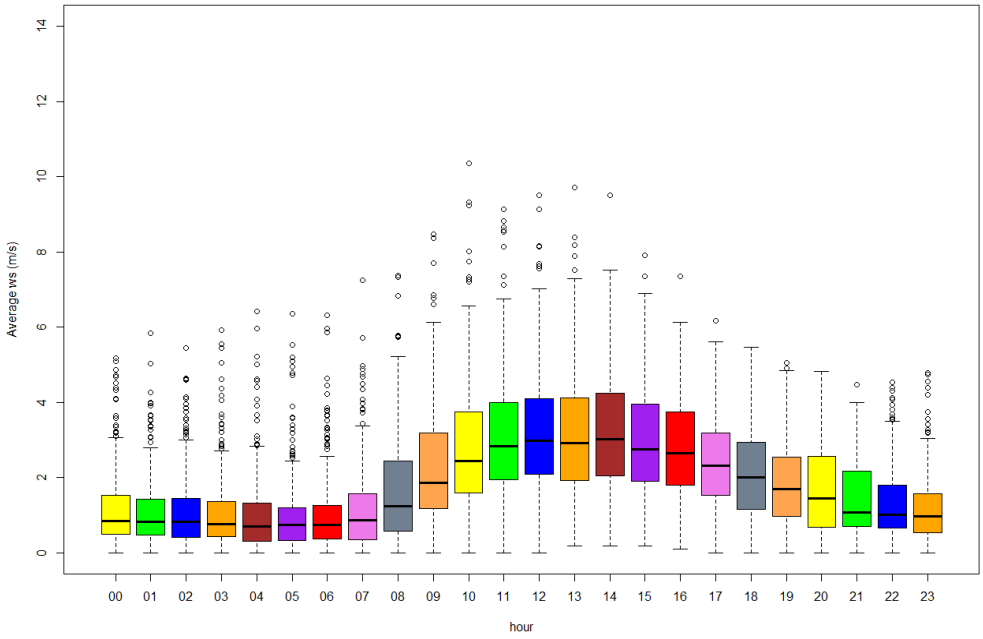

Figure 33: Diurnal wind speed averages for the Sasol Amersfoort Station (whisker & box indicates interquartile range, diamond indicate outliers and the bars indicate the min and max value)

4.1.2.3 POLLUTION ROSES

The pollution rose is useful for considering pollutant concentrations by wind direction, or more specifically the percentage time the concentration is in a particular range. This type of approach can be very informative for air pollutant species (Henry *et al*. 2009).

ESKOM EZAMOKUHLE & MAJUBA STATION

Figures 34 to 42 illustrates the pollution roses for the various pollutants measured at the Eskom Ezamokuhle & Majuba stations. These plots are very useful for understanding which wind directions control the overall mean concentrations. The pollution rose clearly indicates that high episodes of pollutant levels are primarily related to winds from the: west; north-west direction; east; north east and south east direction. A comparison of the annual wind rose for the Eskom Ezamokuhle station (Figure 22) & the Eskom Majuba station (Figure 24) to the pollution roses (Figure 34 to 42) shows higher pollutant concentrations occur at higher wind speeds. Conversely lower wind speeds (Figure 22 & 24) are associated with lower concentrations (Figure 34 to 42). It should be noted that higher wind speeds are typically associated with elevated emissions from tall stack sources whilst low-level emissions behave differently, and higher concentrations would normally be observed during weak-wind conditions.

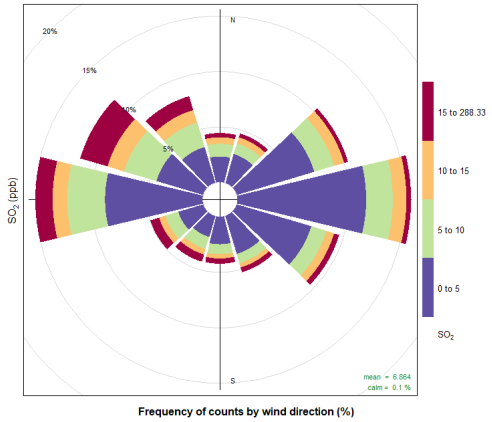

Figure 34: Eskom Ezamokuhle Station pollution rose showing which wind directions contribute most to overall mean concentrations for SO_2

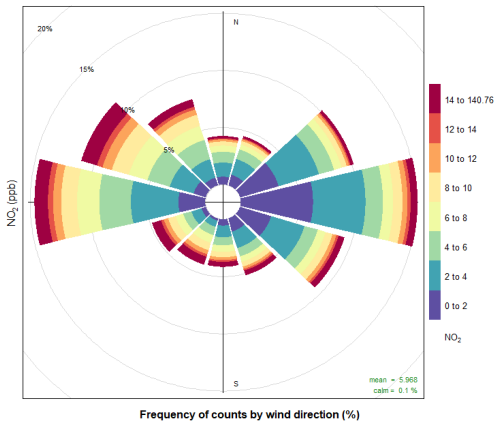

Figure 35: Eskom Ezamokuhle Station pollution rose showing which wind directions contribute most to overall mean concentrations for NO_2

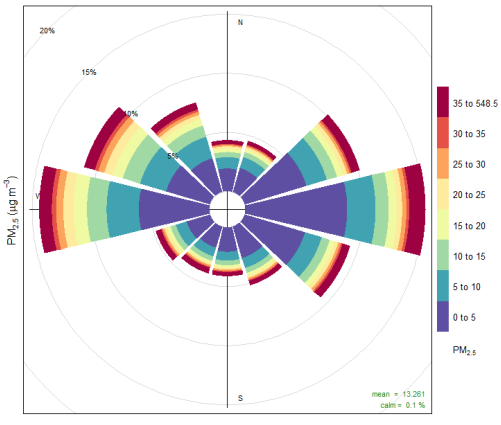

Figure 36: Eskom Ezamokuhle Station pollution rose showing which wind directions contribute most to overall mean concentrations for $PM_{2.5}$

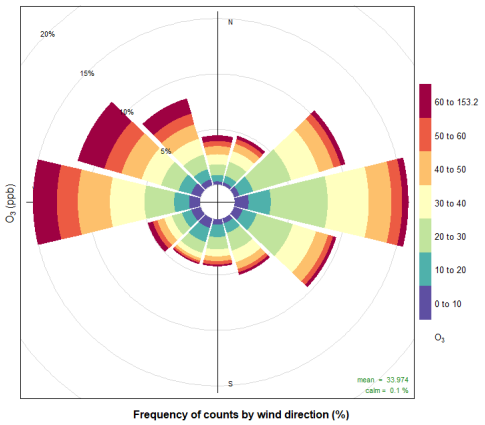

Figure 37: Eskom Ezamokuhle Station pollution rose showing which wind directions contribute most to overall mean concentrations for O_3

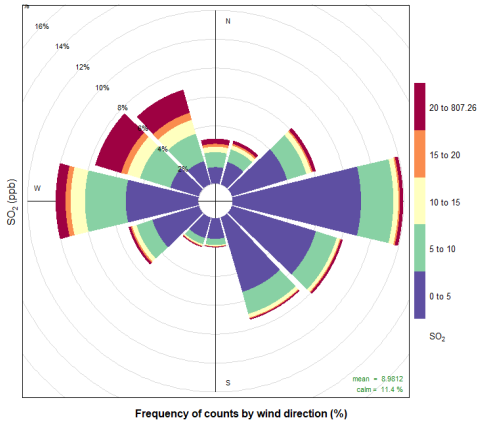

Figure 38: Eskom Majuba Station pollution rose showing which wind directions contribute most to overall mean concentrations for SO_2

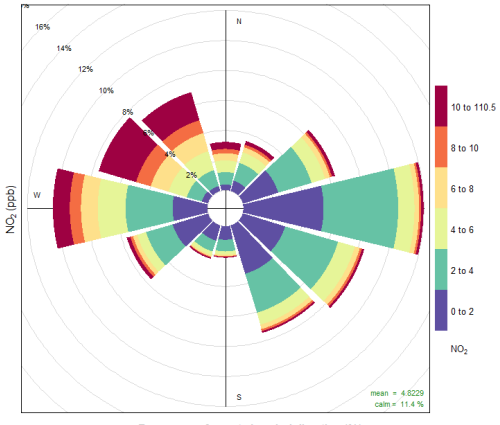

Figure 39: Eskom Majuba Station pollution rose showing which wind directions contribute most to overall mean concentrations for NO_2

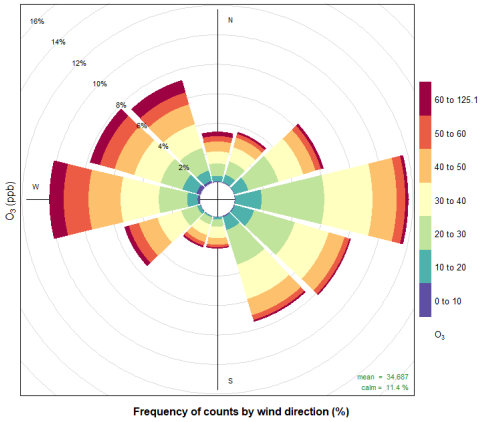

Figure 40: Eskom Majuba Station pollution rose showing which wind directions contribute most to overall mean concentrations for O_3

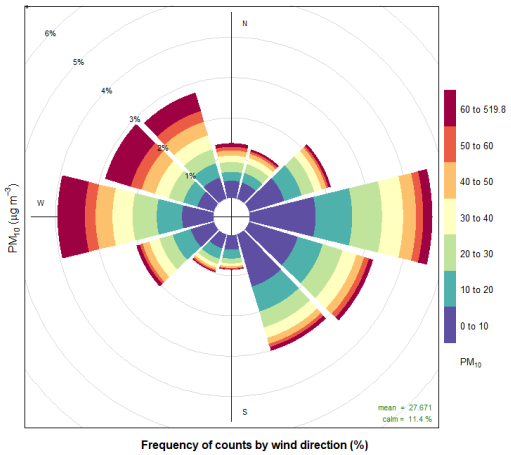

Figure 41: Eskom Majuba Station pollution rose showing which wind directions contribute most to overall mean concentrations for PM_{10}

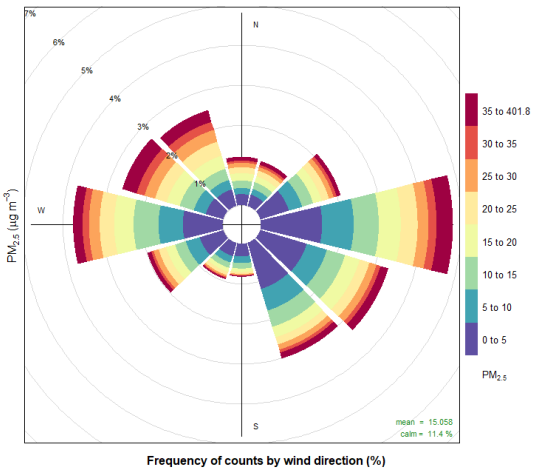

Figure 42: Eskom Majuba Station pollution rose showing which wind directions contribute most to overall mean concentrations for $PM_{2.5}$

SASOL AMERSFOORT STATION

Figures 33 illustrates the pollution rose for H_2S measured at the Sasol Amersfoort station. The pollution rose clearly indicates that high episodes of pollutant levels are primarily related to winds from the: north-west, west and north east. A comparison of the annual wind rose for the Sasol Amersfoort station (Figure 26) to the pollution rose (Figure 43) shows higher pollutant concentrations occur at higher wind speeds. Conversely lower wind speeds (16) are associated with lower concentrations (Figure 43).

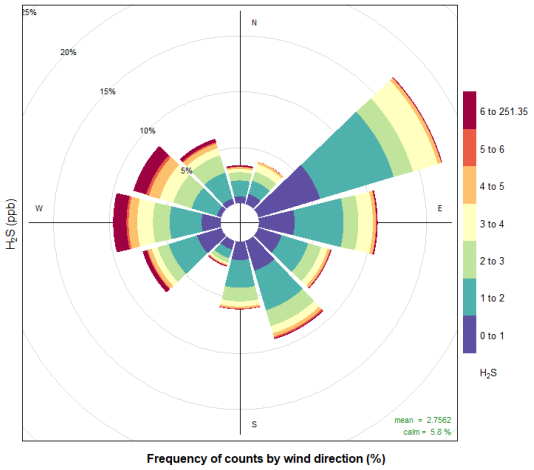

Figure 43: Sasol Amersfoort Station pollution rose showing which wind directions contribute most to overall mean concentrations for H_2S

4.1.3 CORRELATION MATRIX

It's important to understand how how different variables are related to one another. However, it can be difficult to easily develop an understanding of the relationships when many multiple variables are present. A solution herein is to plot a correlation matrix, which provides the correlation between all pairs of data. This helps visualise relationships between variables (Friendly, 2002; Andarkar, 2007).

The correlation matrix shows the correlation coded in three ways: by shape (ellipses), colour and the numeric value. The ellipses can be thought of as visual representations of scatter plot. With a perfect positive correlation a line at 45 degrees positive slope is drawn. For zero correlation the shape becomes a circle (Carlaw, 2015). Figures 44 to 46 illustrates the correlation matrix for the various pollutants measured at the: Eskom Ezamokuhle; Eskom Majuba & Sasol Amersfoort stations.

4.3.1.1 ESKOM EZAMOKUHLE STATION

Correlation matrix between all parameters available for the Eskom Ezamokuhle station (Figure 44) indicates that, the highest correlation coefficient is between NO_2 and SO_2 (r = 0. 74) and that the correlations between O_3 and temperature are also high (r = 0.71). Its noted that for the Eskom Ezamokuhle station the SO_2 (Figure 7) concentrations, show a typical industrial signature with increased SO_2 concentrations as just before midday due to the break-up of an elevated inversion layer.

O_3 is a secondary pollutant formed as a result of photochemical reactions in the presence of sunlight (Tienhoven et al., 2005). O_3 has a negative correlation with most pollutants, which is expected due to the reaction between NO and O_3. The formation of this pollutant during intensive insolation episodes explains the strong positive relationship between O_3 air concentration and temperature.

4.3.1.2 ESKOM MAJUBA STATION

The correlation matrix showing the relationships between variables measured at the Eskom Majuba Station are shown in Figure 45. The highest correlation coefficient is between NO_2 and SO_2 (r = 0. 70) and that the correlations between PM_{10} and $PM_{2.5}$ (r = 0.63) is fairly high. Additionally there is a correlation between O_3 and temperature (r = 0.50).

At the Eskom Majuba station, there is an increased SO_2 and NO_2 concentrations at just before midday due to the break-up of an elevated inversion layer, in addition to the development of daytime convective conditions causing the plume to be brought down to ground level relatively close to the point of release from tall stacks. In terms of the relationship between $PM_{2.5}$ and PM_{10}, it has been proved by numerous studies (Munir et al., 2017; Wang et al., 2014) that the mass concentration of $PM_{2.5}$ is highly correlated with PM_{10} .The bi-modal particulate matter peak for the Eskom Majuba station (Figure 11) is typical with the profile for residential fuel burning. The formation of this O_3 during intensive insolation episodes explains the strong positive relationship between O_3 air concentration and temperature.

4.3.1.3 SASOL AMERSFOORT STATION

Correlation matrix between all parameters available for Sasol Amersfoort station (Figure 46) indicates that, there is a moderate correlation coefficient is between wind speed and temperature (r = 0. 46). According to Thangprasert & Suwanarat (2017) there is a correlation between wind speed and temperature with wind speeds increasing with a greater temperature difference (Figure 33).

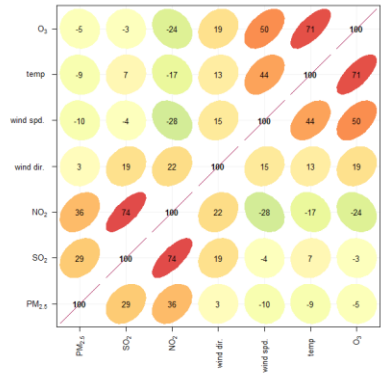

Figure 44: Correlation matrix showing the relationships between variables measured at the Eskom Ezamokuhle Station

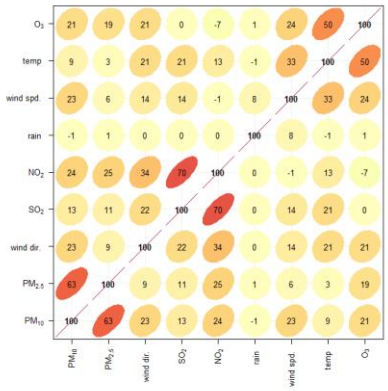

Figure 45: Correlation matrix showing the relationships between variables measured at the Eskom Majuba Station

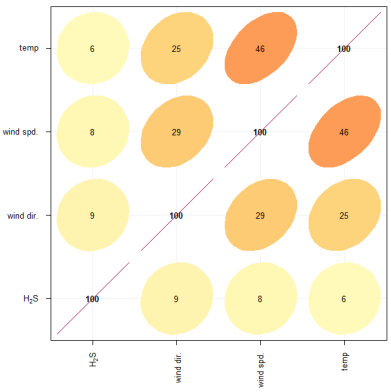

Figure 46: Correlation matrix showing the relationships between variables measured at the Sasol Amersfoort Station

4.2 EMISSION SOURCE CONTTRIBUTION

The emission performance of an individual air-pollution source can be inferred from an ambient record by isolating its signal of impacts. However, ambient data are not conventionally used for such purposes because individual signals tend to be modified, obscured or complicated by confounding factors (Szulecka et al., 2017). However, more detailed and source-specific information can be extracted if analyses are performed using a subset of the data that has been 'conditionally-selected' to exclude superimposed impacts from non-relevant sources (Malby et al., 2013). Numerous studies (Carslaw, 2007; Griffin et al., 2009; Malby et al., 2008; Shu et al., 2017) have demonstrated that these signals can successfully be used for source attribution. A common method for source characterisation is the use of bivariate polar plots (Carslaw et al., 2006; Westmoreland et al., 2007; Carslaw and Beevers, 2013; Uria Tellaetxe and Carslaw, 2014).

4.2.1 Bivariate Polar Plots

Bivariate polar plots have proved to be extremely valuable for identifying and understanding sources of air pollution (Carslaw et al., 2006; Westmoreland et al., 2007). Bivariate polar plots provide an effective graphical means of discriminating different source types and characteristics as these plots show how the concentration of a pollutant varies by two different variables at a specific receptor.

4.2.1.1 Bivariate Polar Plot for Mean Concentration

These plots show how the concentration of a pollutant varies by wind direction and wind speed at a receptor. The wind speed dependence of a source can provide important information concerning the source type and characteristics (Carslaw et al., 2006; Jones et al., 2010). High ground level concentrations from tall stack emissions are more prevalent during stronger wind speeds during stable conditions whilst conversely low-level emissions, and higher concentrations would normally be observed during weak-wind conditions.

Eskom Ezamokuhle Station

Figures 47 to 50 shows the bivariate plots for the Eskom Ezamokuhle station conditioned for the mean pollutant concentration. The SO_2 concentrations observed at the station (Figure 47) show two distinct wind directions, namely from the south-west and the north-west. High concentrations present at high wind speeds are indicative of emissions from stacks rather than non-buoyant ground-level sources. Hence the higher SO_2 concentrations associated with the south-westerly winds are most likely due to emissions from the Eskom Majuba station (Figure 7). Similarly the SO_2 concentrations from the north-

west indicates a distinct tall stack emission source and this corresponds to the exact direction of a significant petrochemical facility located in Secunda which may be the likely emission source.

Figure 48 shows the bivariate NO_2 polar plot for the Eskom Ezamokuhle station. The highest concentrations occur under very low wind speed conditions from the south-west. These high concentrations occur under stable atmospheric conditions when non-buoyant ground-level sources are important such as road transport emissions. Figure 7 confirms that these NO_2 concentrations are the likely impact of vehicle emissions. The bivariate polar plot also shows are area of high concentration to the north-west that occur at high wind speeds, possibly corresponding to the activities of a petrochemical facility located in Secunda.

Elevated particulate concentrations at Ezamokuhle show contributions from the north-west and the south-east at higher (between 8 and 14 m/s) wind speeds (Figure 49). At low wind speeds the symmetrical plot shows a localised contribution, most likely the result of residential fuel burning (Figure 10). Additionally elevated O_3 concentrations (Figure 50) are shown to occur under high wind speed conditions from all wind directions where the source of O_3 is not clear.

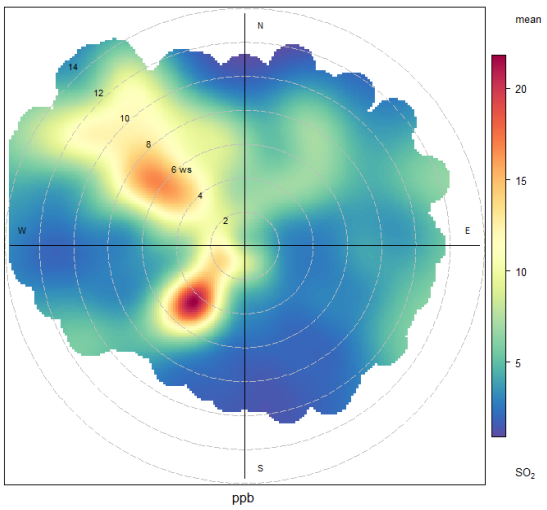

Figure 47: Polar plot of hourly mean SO_2 concentration at the Eskom Ezamokuhle Station for 2018 to 2020

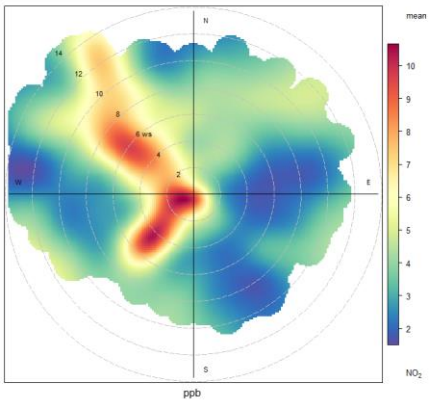

Figure 48: Polar plot of hourly mean NO_2 concentration at the Eskom Ezamokuhle Station for 2018 to 2020

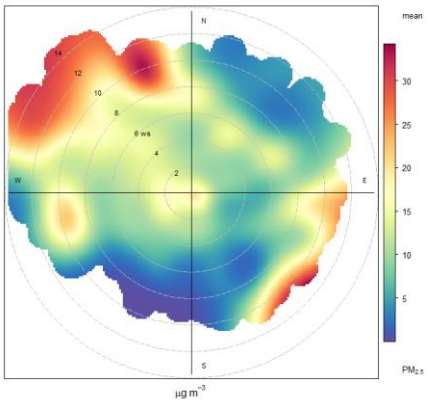

Figure 49: Polar plot of hourly mean $PM_{2.5}$ concentration at the Eskom Ezamokuhle Station for 2018 to 2020

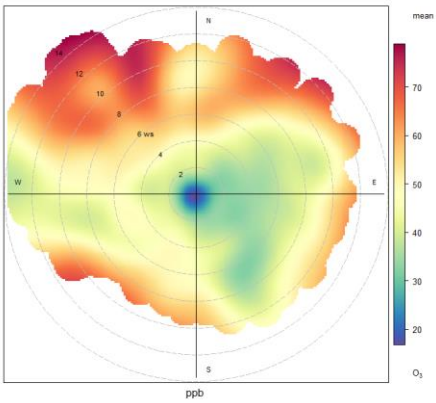

Figure 50: Polar plot of hourly mean O_3 concentration at the Eskom Ezamokuhle Station for 2018 to 2020

ESKOM MAJUBA STATION

The SO_2 (Figure 51) and NO_2 (Figure 52) concentrations observed at the Eskom Majuba station clearly show that the highest SO_2 and NO_2 concentrations occur when the wind is blowing from the north-west. The high concentrations occur under very high wind speeds conditions (between 6 to 15 m/s) from the north-west which is most likely due to emissions from the Eskom Majuba station (Figure 8). Elevated particulate concentrations (Figure 53) at the Eskom Majuba station show contributions from both the east and west at higher wind speeds (between 12 and 16 m/s). At low wind speeds the symmetrical plot shows a localised contribution, most likely the result of residential fuel burning (Figure 11). Peak O_3 concentrations (Figure 54) are shown to occur under high wind speed conditions from the north-west and south-west where the source of O_3 is not clear.

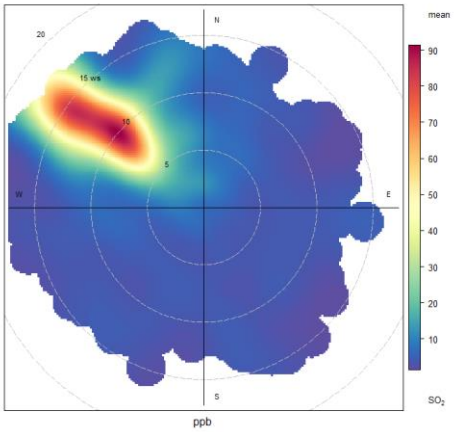

Figure 51: Polar plot of hourly mean SO_2 concentration at the Eskom Majuba Station for 2018 to 2020

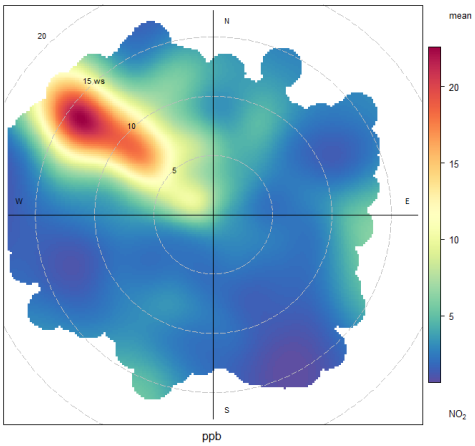

Figure 52: Polar plot of hourly mean NO_2 concentration at the Eskom Majuba Station for 2018 to 2020

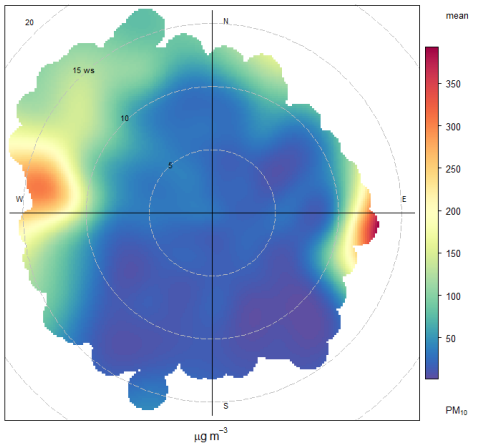

Figure 53: Polar plot of hourly mean PM_{10} concentration at the Eskom Majuba Station for only 2018

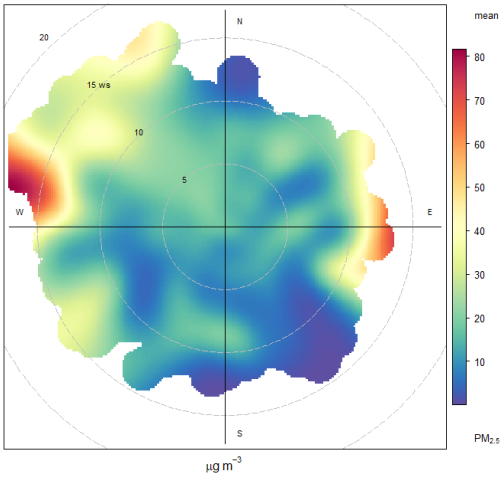

Figure 54: Polar plot of hourly mean $PM_{2.5}$ concentration at the Eskom Majuba Station for only 2018

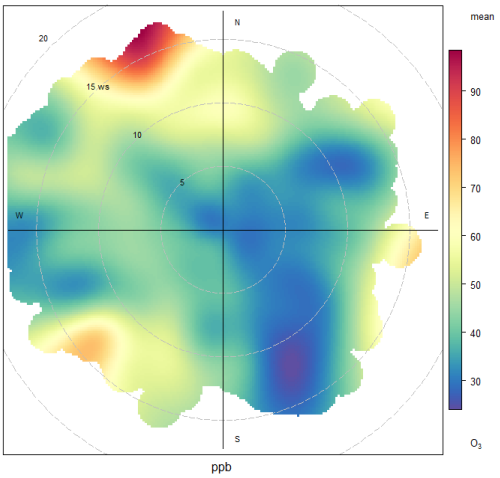

Figure 55: Polar plot of hourly mean O_3 concentration at the Eskom Majuba Station for 2018 to 2020

SASOL AMERSFOORT STATION

Figure 53 clearly shows that the highest H_2S concentrations occur when the wind is blowing from the north-west. These high H_2S concentrations from the north-west occur under high wind speed conditions indicating a distinct tall stack emission source which corresponds to the exact direction of a significant petrochemical facility located in Secunda which is the likely emission source.

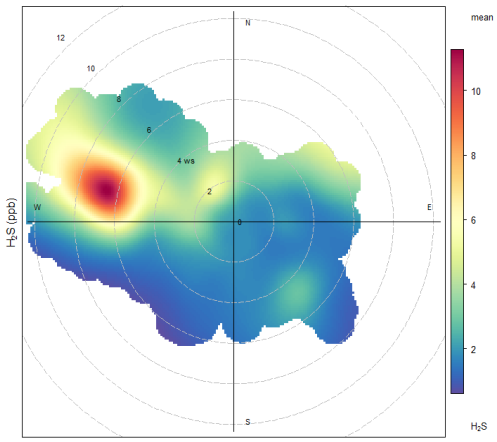

Figure 56: Polar plot of hourly mean H_2S concentration at the Sasol Amersfoort Station for 2018 to 2020

4.2.1.2 BIVARIATE POLAR PLOT FOR MEAN CONCENTRATION & TEMPERATURE

These plots show how the concentration of a pollutant varies by wind direction and temperature at a receptor. Temperature can help reveal high-level sources brought down to ground level in unstable atmospheric conditions, or show the effect a source emission dependent on temperature e.g. residential burning for space heating.

ESKOM EZAMOKUHLE STATION

Figures 57 and 58 shows the bivariate polar plot for SO_2 & NO_2 concentrations as a function of wind direction and surface temperature. It is apparent that there is a clear dependence of both SO_2 and NO_2 concentrations with increasing ambient temperature. The reason why concentrations increase with increasing temperature is that dispersing plumes from tall stacks are brought down to ground level under unstable atmospheric conditions when thermal turbulence is increased. However, for NO_2, elevated concentrations are observed at lower temperatures as well, which points to the influence of road transport throughout the year (Figure 7). For particulates (Figure 59) the highest concentrations

occur during low temperatures, which results mostly from residential fuel burning in winter (Figure 19). O_3 in the lower troposphere forms through the reaction between oxides of nitrogen and volatile organic compounds in the presence of the ultraviolet portion of sunlight. Thus the formation of O_3 during intensive insolation episodes explains the strong positive relationship between O_3 air concentration and increased surface temperature (Figure 60).

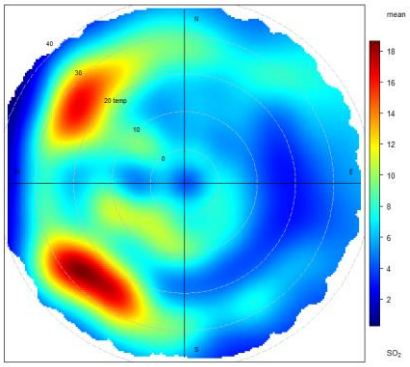

Figure 57: Polar plot function for the mean SO_2 concentration plotted against temperature at the Eskom Ezamokuhle Station for 2018 to 2020

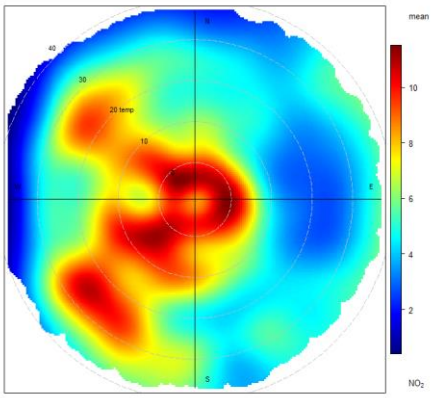

Figure 58: Polar plot function for the mean NO_2 concentration plotted against temperature at the Eskom Ezamokuhle Station for 2018 to 2020

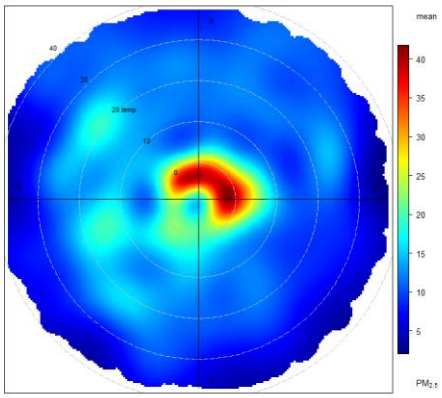

Figure 59: Polar plot function for the mean $PM_{2.5}$ concentration plotted against temperature at the Eskom Ezamokuhle Station for 2018 to 2020

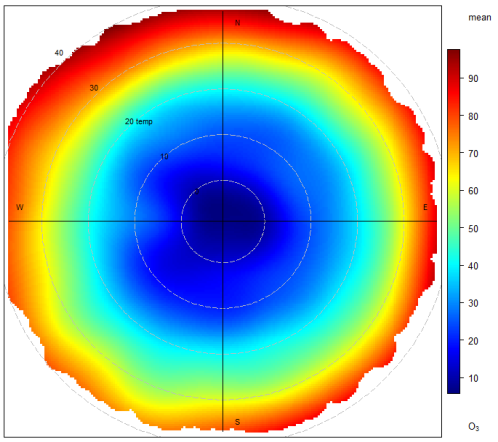

Figure 60: Polar plot function for the mean O_3 concentration plotted against temperature at the Eskom Ezamokuhle Station for 2018 to 2020

ESKOM MAJUBA STATION

Figures 61 to 64 shows the bivariate polar plot for SO_2,NO_2, PM_{10} and $PM_{2.5}$ concentrations its apparent that there is a clear dependence of SO_2,NO_2, PM_{10} and $PM_{2.5}$ peak concentrations with increasing ambient temperature. This is due to the dispersing plumes from the tall stacks (likely Majuba Power Station) & brought down to ground level under unstable atmospheric conditions when thermal turbulence is increased (Figure 8). Additionally for PM_{10} and $PM_{2.5}$ (Figure 63 & 64) lower localised concentrations occur during low temperatures, which results mostly from residential fuel burning in winter (Figure 20). The formation of O_3 during intensive insolation episodes explains the strong positive relationship between O_3 air concentration and increased surface temperature (Figure 65).

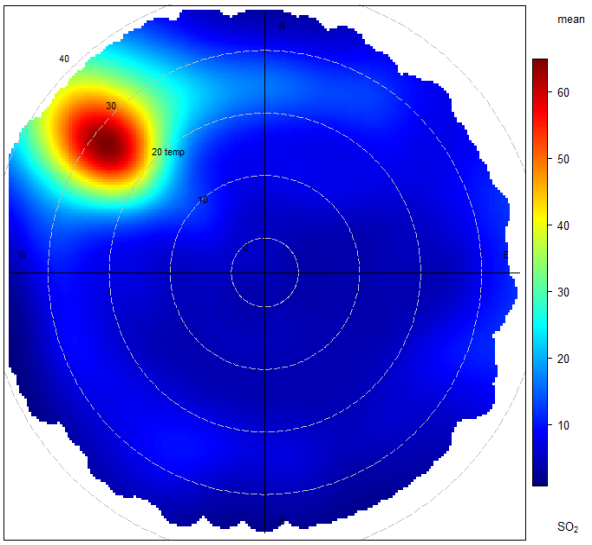

Figure 61: Polar plot function for the mean SO_2 concentration plotted against temperature at the Eskom Majuba Station for 2018 to 2020

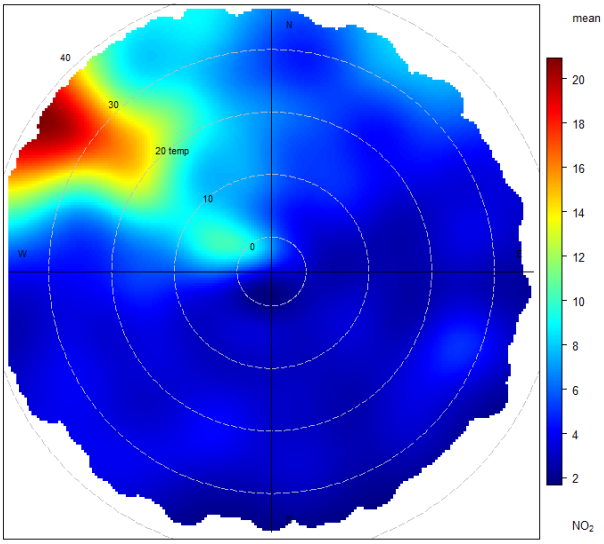

Figure 62: Polar plot function for the mean NO_2 concentration plotted against temperature at the Eskom Majuba Station for 2018 to 2020

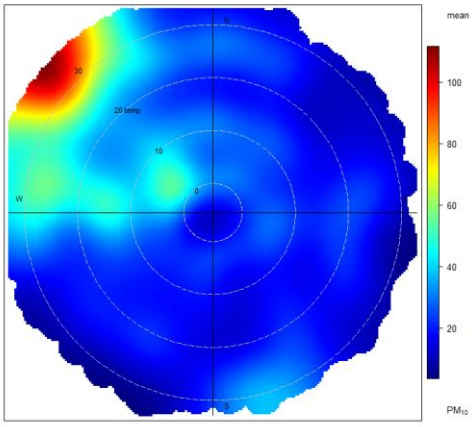

Figure 63: Polar plot function for the mean PM_{10} concentration plotted against temperature at the Eskom Majuba Station for 2018

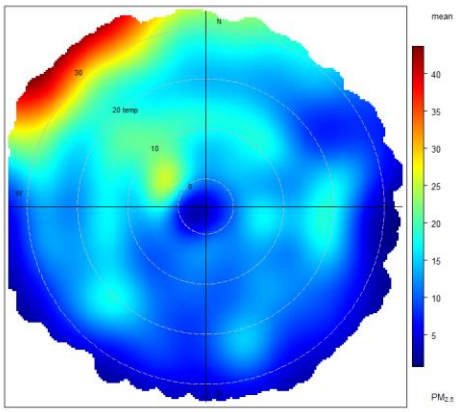

Figure 64: Polar plot function for the mean $PM_{2.5}$ concentration plotted against temperature at the Eskom Majuba Station for 2018

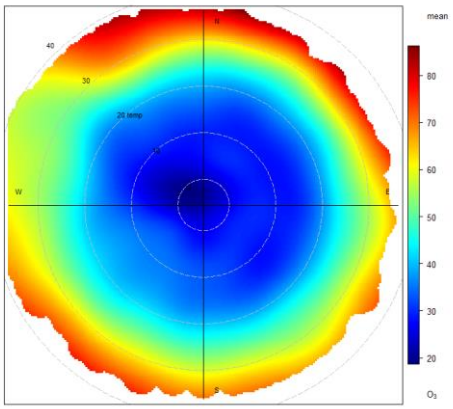

Figure 65: Polar plot function for the mean O3 concentration plotted against temperature at the Eskom Majuba Station for 2018 to 2020

SASOL AMERSFOORT STATION

Figures 66 shows the bivariate polar plot for H_2S concentrations wherein it's apparent that there is a clear dependence of the H_2S peak concentrations with increasing ambient temperature. This is due to the dispersing plumes from the tall stacks (likely petrochemical facility in Secunda) which is brought down to ground level under unstable atmospheric conditions when the thermal turbulence is increased (Figure 9).

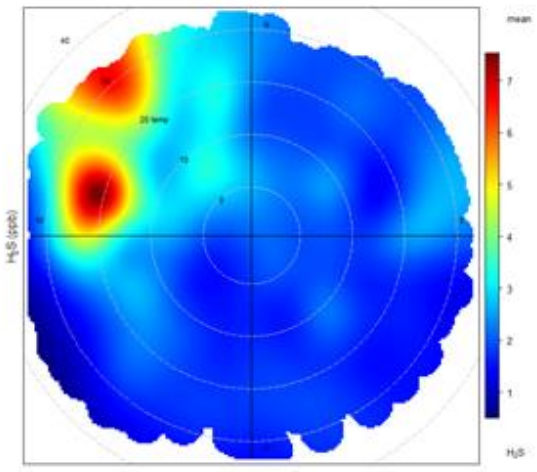

Figure 66: Polar plot function for the mean H_2S concentration plotted against temperature at the Sasol Amersfoort Station for 2018 to 2020

4.4 EVALUTION OF DATA TO NAAQS COMPLIANCE

In South Africa ambient air quality is regulated by AQA through compliance with health-based ambient air quality standards (NAAQS) as presented in Table 1. The frequency of permissible exceedances (FoE) for the NAAQS are shown in Table 7. A summary of the ambient data measured at the Eskom Ezmokuhle and Eskom Majuba station's for the period 2018 – 2020 is provided in Table 8. It must be noted that South Africa currently does not have a NAAQS for H_2S hence the Sasol Amersfoort station which measures only H_2S is excluded from the evaluation herein.

Table 7: Permissible FoE of the NAAQS for SO_2, NO2, PM_{10} & $PM_{2.5}$

Pollutant	SO_2		NO_2	PM_{10}	$PM_{2.5}$
Period	**Hourly**	**Daily**	**Hourly**	**Daily**	**Daily**
Permissible FoE for NAAQS	88	4	88	4	4

Table 8: Frequency of exceedance of the NAAQS pollutant limit value at the Eskom Ezamokuhle and Eskom Majuba station for the period 2018 to 2020

Station	Year	Actual number of recorded FoE of the NAAQS limit value				
		SO_2		NO_2	PM_{10}	$PM_{2.5}$
		Hourly	Daily	Hourly	Daily	Daily
Ezamokhule	**2018**	3	0	0	Not Measured	1
	2019	0	0	0		**5***
	2020	0	0	0		**50***
Majuba	**2018**	12	0	0	**25***	**5***
	2019	21	1	0	Not Measured	
	2020	0	0	0		

*Exceedances are shown in red text

4.4.1 Eskom Ezamokuhle Station

The time-series graphs (Figure 67 to 71) summarise the observed concentrations of SO_2, NO_2, and $PM_{2.5}$ at the Eskom Ezamokuhle monitoring station for the years 2018 to 2020. The hourly 99th percentiles for SO_2 were only above the limit value of 134 ppb for 3 occasions in 2018 (Figure 67). These exceedance occur in the months of January, April and August just around midday. These peak concentrations for these periods corresponds to the trend level plot (Figure 14) for the station which also indicate that the timing of peak concentrations occur at midday. Additionally the polar plot for the station (Figure 47) further show a typically industrial signature with increased SO_2 concentrations as just before midday due to the break-up of an elevated inversion layer, in addition to the development of daytime convective conditions causing the plume to be brought down to ground level relatively close to the point of release from tall stacks. Thus these exceedances are likely due to the impact of an elevated emission source. It's evident from Figures 68 that the daily SO_2 concentrations were well below the NAAQS limit value of 48 ppb for the entire period. Similarly Figure 68 clearly shows that there were no recorded exceedances of the hourly NO_2 NAAQS standard of 106 ppb.

The NAAQS for the daily $PM_{2.5}$ limit (40 ug/m3) was exceeded for 1 occasion in 2018 (Figure 70). The 2018 calendar $PM_{2.5}$ plot (Figure 70) for the Eskom Ezamokuhle station indicates that on the

Sunday 29th July 2018 an elevated $PM_{2.5}$ concentration of 61µg/m^3 was recorded. This peak concentration occurs at 7pm thus indicating the impact of a residential fuel burning source (Figure 10 & 19).

For 2019, the NAAQS for the daily $PM_{2.5}$ limit was exceeded on 5 occasions (Figure 70). The 2019 calendar $PM_{2.5}$ plot (Figure 72) indicates that the NAAQS for $PM_{2.5}$ was exceeded in the months of June and July only. The 2019 trend level plot for $PM_{2.5}$ (Figure 19) further indicates that for these winter months, peak concentrations of $PM_{2.5}$ occurs at 08:00 whilst the evening peak occurs at 18:00, a typical profile for residential fuel burning.

In 2020, 50 NAAQS exceedances of the daily $PM_{2.5}$ limit were measured (Figure 70). It's evident from the 2020 calendar plot (Figure 73) that the NAAQS for $PM_{2.5}$ was exceeded in the months of July and December. Similarly to the $PM_{2.5}$ exceedance recorded for both 2018 & 2019, the highest concentrations occur during low temperatures in July 2020, which results from residential fuel burning in winter. A comparison of the trend level plot for the Eskom Ezamokuhle station (Figure 19) shows that for December 2020, these emissions occur between 17:00 to 21:00 with emissions peaking at 18:00 thus indicating the impact of a residential fuel burning source.

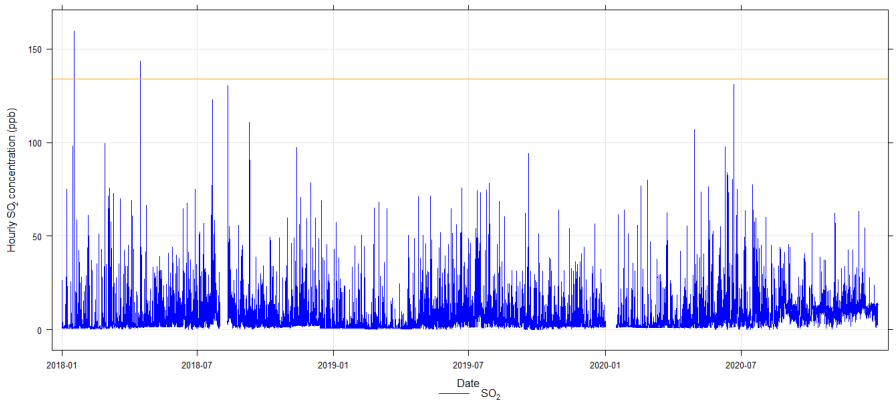

Figure 67: Time series for the hourly SO_2 ground level concentrations measured at the Eskom Ezamokuhle ambient air quality monitoring station (2018-2020)

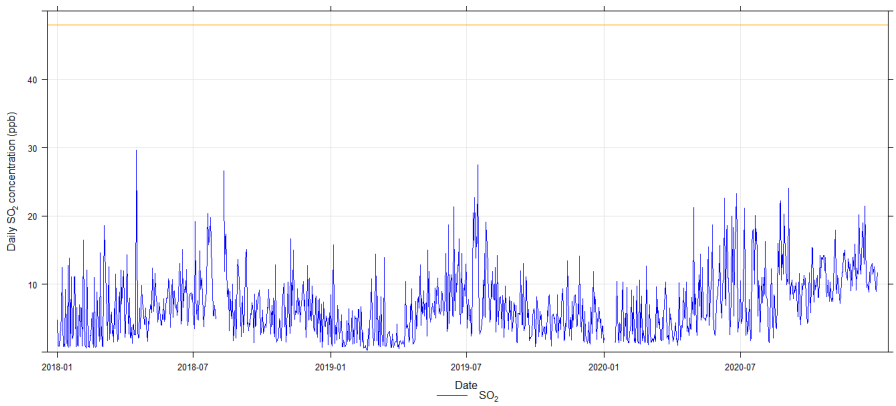

Figure 68: Time series for the daily SO_2 ground level concentrations measured at the Eskom Ezamokuhle ambient air quality monitoring station (2018-2020)

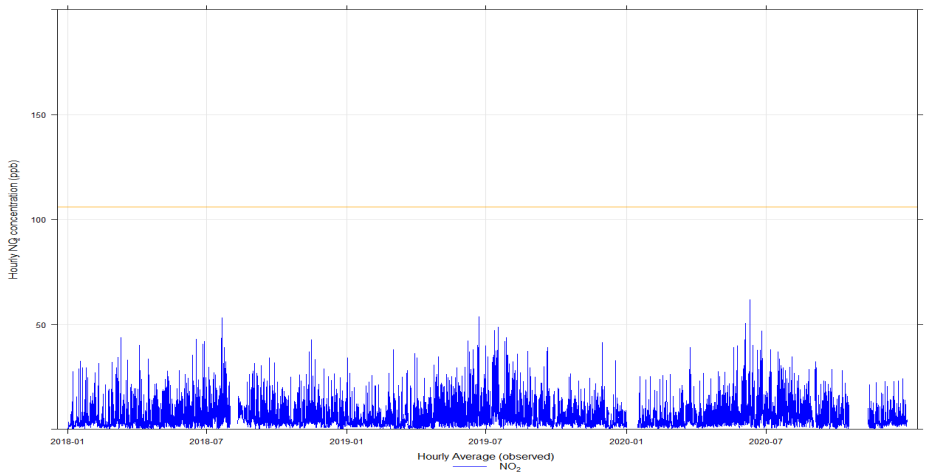

Figure 69: Time series for the hourly NO_2 ground level concentrations measured at the Eskom Ezamokuhle ambient air quality monitoring station (2018-2020)

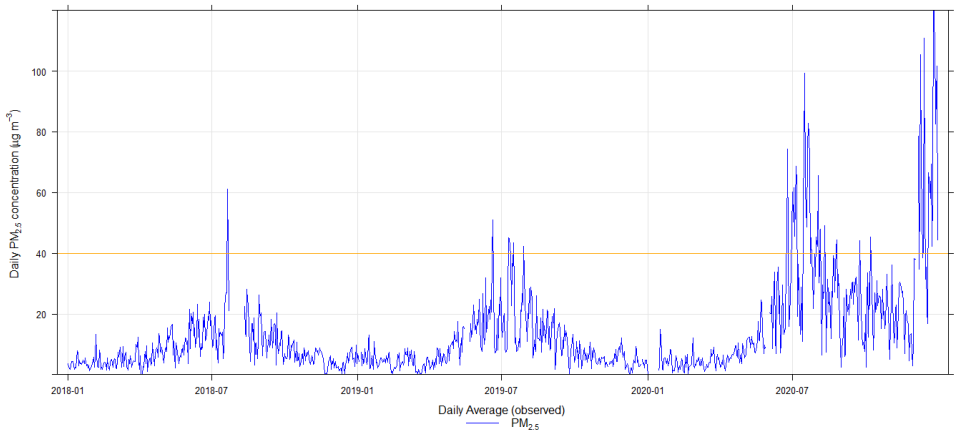

Figure 70: Time series for the daily $PM_{2.5}$ ground level concentrations measured at the Eskom Ezamokuhle ambient air quality monitoring station (2018-2020)

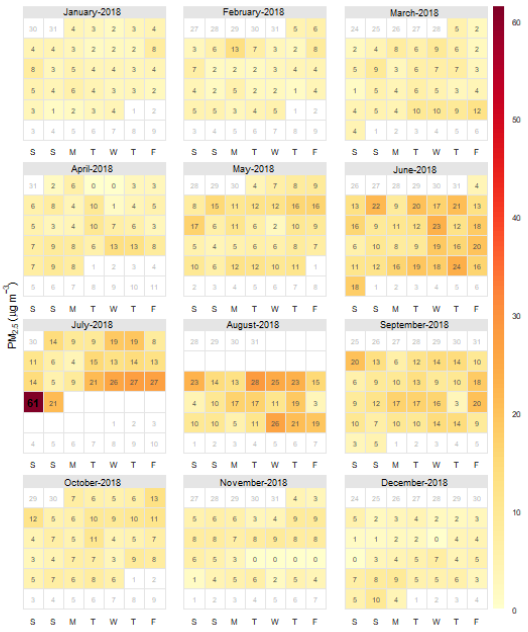

Figure 71: Calendar plot for the daily $PM_{2.5}$ ground level concentrations measured at the Eskom Ezamokuhle ambient air quality monitoring station for 2018

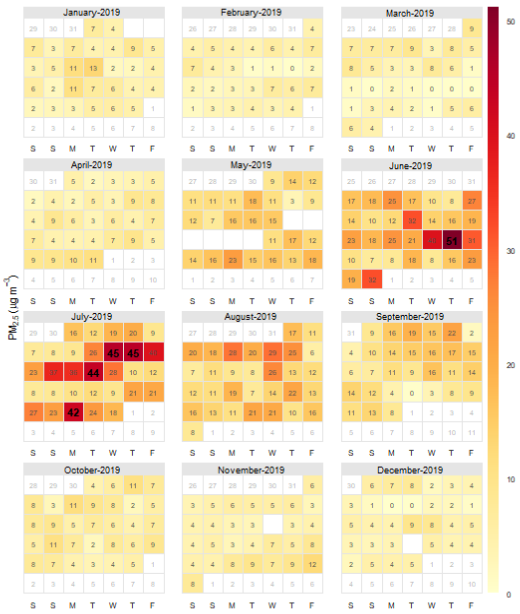

Figure 72: Calendar plot for the daily $PM_{2.5}$ ground level concentrations measured at the Eskom Ezamokuhle ambient air quality monitoring station for 2019

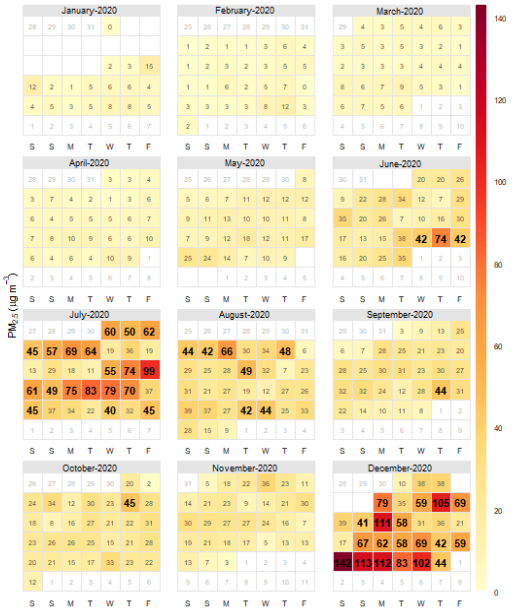

Figure 73: Calendar plot for the daily $PM_{2.5}$ ground level concentrations measured at the Eskom Ezamokuhle ambient air quality monitoring station for 2020

4.4.2 ESKOM MAJUBA STATION

The time-series graphs (Figure 74 to 78) summarise the observed concentrations of SO_2, NO_2, PM_{10} and $PM_{2.5}$ at the Eskom Ezamokuhle monitoring station for the years 2018 to 2020.

For 2018 there was 12 exceedances of the hourly SO_2 NAAQS (134 ppb) whilst in 2019, 21 exceedances were recorded (Table 8). These peak concentrations occur in the months of March, August, September and November (Figures 15 and 74). The trend level plot (Figure 15) for the station indicates that the timing of these peak concentrations occur around midday. This is typical of industrial signature with increased SO_2 concentrations as just before midday due to the rising of the elevated inversion layer, in addition to the development of daytime convective conditions causing the plume to be brought down to ground level relatively close to the point of release from tall stacks. The pollution rose for Eskom Majuba Station (Figure 24) shows that evaluated SO_2 concentrations are present at the station during high wind speed conditions which is further indicative of emissions from stacks rather than non-buoyant ground-level sources. Additionally the polar plot for the mean hourly SO_2 concentration (Figure 51) observed at the Eskom Majuba Station show that the highest SO_2 concentrations occur when the wind is blowing from the north-west which is most likely due to emissions from the Eskom Majuba station.

Figure 75 illustrates that the daily SO_2 concentrations were well below the NAAQS limit value of 48 ppb for 2018 whilst for 2019 one exceedance was recorded (Figure 79). Figure 75 clearly shows that there were no recorded exceedances of the hourly NO_2 NAAQS standard of 106 ppb for the entire period (2018 to 2020).

In terms of the relationship between $PM_{2.5}$ and PM_{10}, it has been proved by numerous studies (Munir et al., 2017; Wang et al., 2014) that the mass concentration of $PM_{2.5}$ is highly correlated with PM_{10}. The correlation coefficient between PM_{10} and $PM_{2.5}$ for the Eskom Majuba station is fairly high (Figure 45). The 2018 calendar PM_{10} and $PM_{2.5}$ plots (Figure 82 & 83) illustrate that peak concentrations occur in the months of June, July, August, September and October. For 2018 there 25 exceedances of the daily PM_{10} limit (75 ug/m^3) and 5 exceedances of the daily $PM_{2.5}$ limit (40 ug/m^3). It's evident from the 2018 PM_{10} and $PM_{2.5}$ trend level plots (Figures 20 & 21) that that the timing of these peak concentrations corresponds to a typical profile for residential fuel burning. Additionally the bi-modal particulate matter peaks (Figure 11) further confirms residential fuel burning as the source herein.

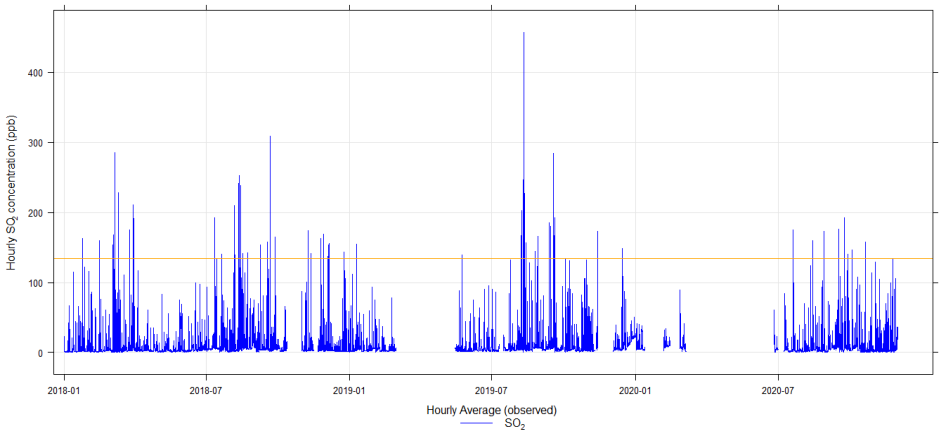

Figure 74: Time series for the hourly SO_2 ground level concentrations measured at the Eskom Majuba ambient air quality monitoring station (2018-2020)

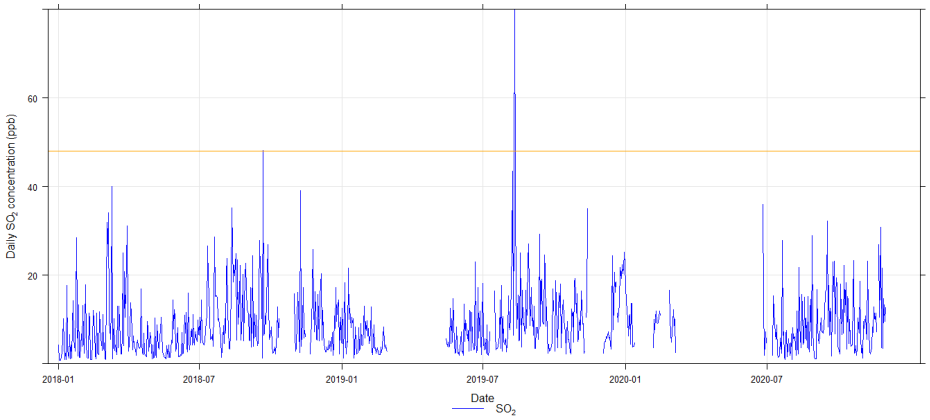

Figure 75: Time series for the daily SO_2 ground level concentrations measured at the Eskom Majuba ambient air quality monitoring station (2018-2020)

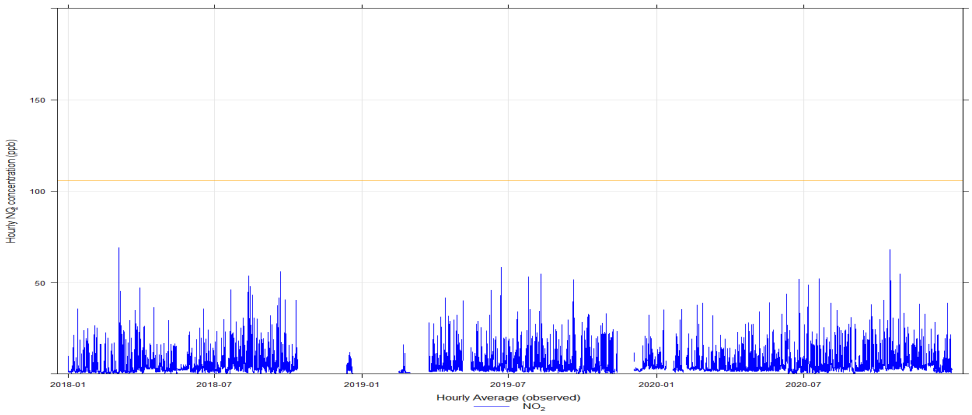

Figure 76: Time series for the hourly NO_2 ground level concentrations measured at the Eskom Majuba ambient air quality monitoring station (2018-2020)

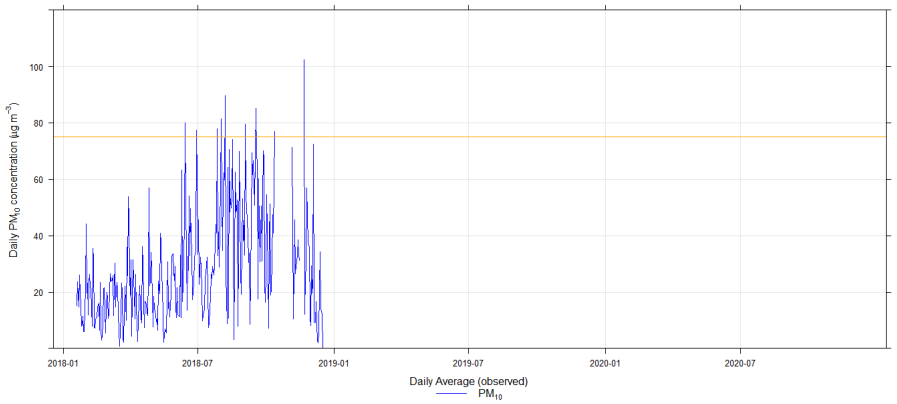

Figure 77: Time series for the daily PM_{10} ground level concentrations measured at the Eskom Majuba ambient air quality monitoring station (only for 2018)

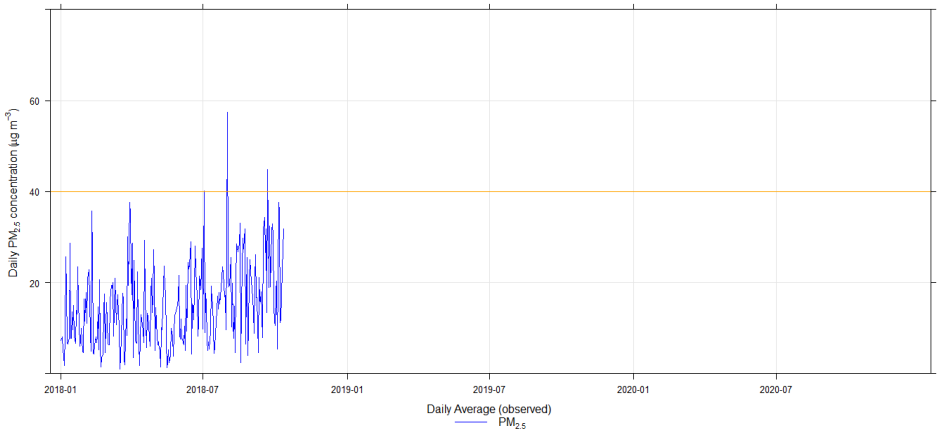

Figure 78: Time series for the daily $PM_{2.5}$ ground level concentrations measured at the Eskom Majuba ambient air quality monitoring station (only for 2018)

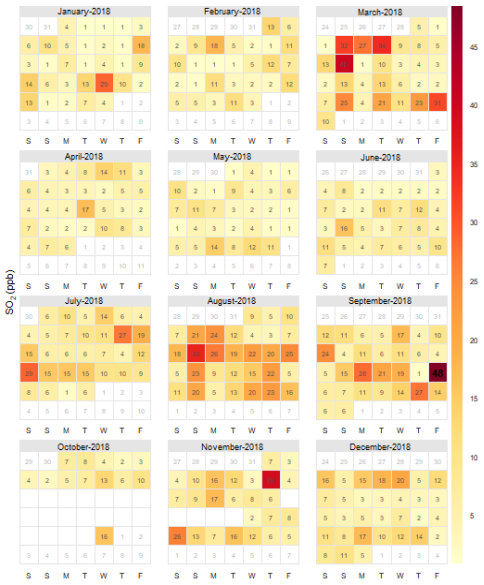

Figure 79: Calendar plot for the daily SO_2 ground level concentrations measured at the Eskom Majuba ambient air quality monitoring station for 2018

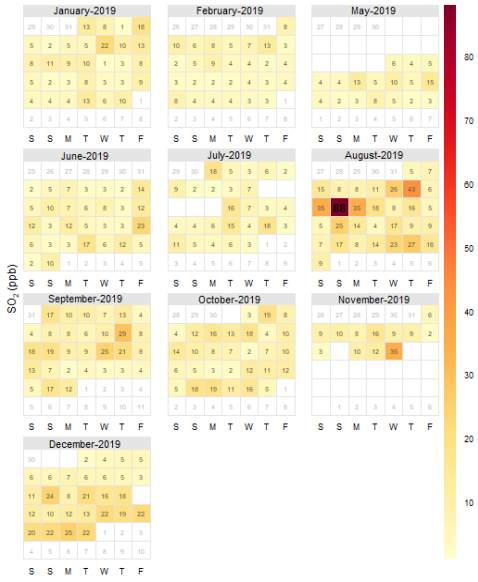

Figure 80: Calendar plot for the daily SO_2 ground level concentrations measured at the Eskom Majuba ambient air quality monitoring station for 2019

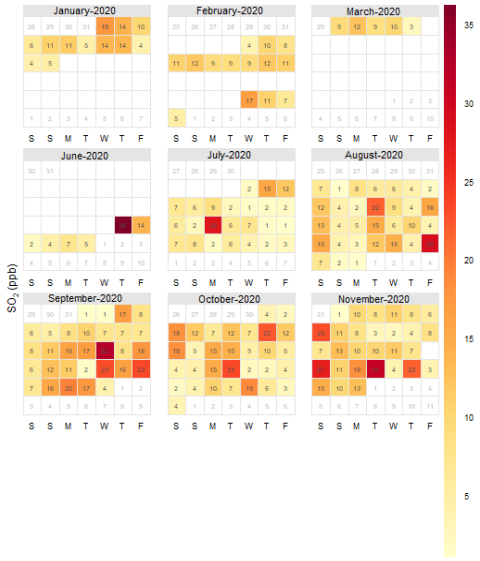

Figure 81: Calendar plot for the daily SO_2 ground level concentrations measured at the Eskom Majuba ambient air quality monitoring station for 2020

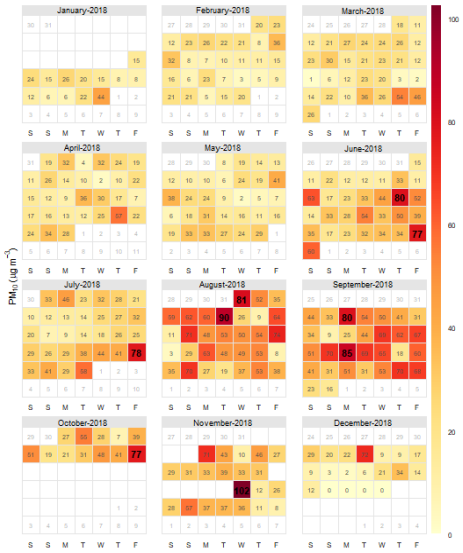

Figure 82: Calendar plot for the daily PM_{10} ground level concentrations measured at the Eskom Majuba ambient air quality monitoring station for 2018

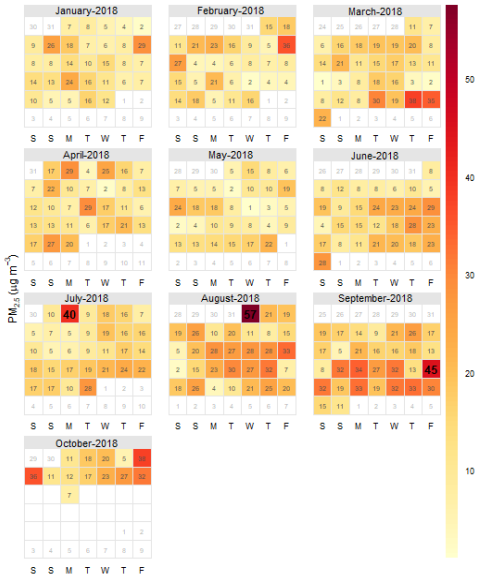

Figure 83: Calendar plot for the daily $PM_{2.5}$ ground level concentrations measured at the Eskom Majuba ambient air quality monitoring station for 2018

4.5 TRAJECTORY ANALYSIS

Trajectories are defined as the paths of infinitely small particles of air (Dutton, 1986). While forward trajectories describe where a particle will go, backward trajectories indicate where it came from. Back trajectory modelling was undertaken using the Hybrid Single-Particle Lagrangian Integrated Trajectory (HYSPLIT) model.

4.5.1 HYSPLIT MODEL

Traditionally, the modelling of atmospheric transport has been accomplished using either an Eulerian or a Lagrangian framework (Stein et al., 2000). The technique employed by the HYSPLIT model calculation is a hybrid between the two approaches (Draxler and Hess, 1998; Heffter, 2002; Rolph et al., 1992; 1993; Stein et al., 2000), hence the "hybrid" component of the acronym refers to the application of both 'Lagrangian' and 'Eulerian' modelling frames of reference within the system (Draxler, 1999a). The HYSPLIT model is designed for computing simple air trajectories to highly elaborate dispersion and deposition simulations (Draxler, 1999b; Draxler and Hess, 1997; Heffter, 2002).

4.5.2 HYSPLIT WINTER CASE STUDY

The HYSPLIT model was utilised to analyse back trajectories for three specific days in winter where the NAAQS for $PM_{2.5}$ was exceeded at the Eskom Ezamokuhle station. These three days were selected based on the highest $PM_{2.5}$ concentrations measured at the Eskom Ezamokuhle station for the period 2018 to 2020. A comparison of the calendar plots (Figure 71 to 73) indicates that the three highest winter $PM_{2.5}$ concentrations were recorded on 17th July 2020 (99 ug/m^3); 21st July 2020 (83 ug/m^3) and 22nd July 2020 (79 ug/m^3). Hence HYSPLIT was simulated for these three days.

4.5.3 HYSPLIT SIMULATION

The meteorological fields used in the HYSPLIT model are four dimensional gridded fields from the National Centre for Environmental Prediction (NCEP). HYSPLIT calculates trajectories using various meteorological forecast models. In this study, the trajectory simulations are undertaken with GFS (0.25 degrees) meteorological data at a 3 hour temporal resolution. For this study, 24-hour kinematic back trajectories were computed from the Eskom Ezamokuhle Station (27.00 S & 29.85 E), at three heights (200m, 500m and 1000m) above ground level (AGL). The kinematic approach was used as the meteorological model generates three-dimensional velocity fields that take diabatic and adiabatic factors into account (Draxler, 1996).

4.5.4 HYSPLIT OUTPUT

The back trajectory maps produced by the HYSPLIT model depict the general path taken by air parcels before reaching their point of origin. The aerial view (top panel) shows the horizontal movement of air parcels while the vertical view (bottom panel) shows the vertical movement of air parcels (Figures 84 to 86). Height is given in meters above ground level.

The 24-hour back trajectory results for 17th July 2020 are shown in Figures 84 & 87. The distinguishing feature in terms of the source region of air masses is that all the trajectories (red, blue and green) originate from a southerly direction from KwaZulu-Natal. There is evidence of relatively light winds associated with the near-surface air (red & blue trajectories) originating in the vicinity of Dundee and stronger southerly winds associated with the higher-surface air (green trajectory) originating in the vicinity of Port Sheptsone as indicated by the difference in the length of daily trajectories. It is interesting to note that higher-surface (green trajectory) air flows directly over the Eskom Majuba Power Station prior to arriving at Ezamokuhle.

For 21st July 2020, the 24-hour back trajectory results are shown in Figures 85 & 88. The distinguishing feature in terms of the source region of air masses is that all the trajectories (red, blue and green) originate from a southerly direction in Kwa-Zulu Natal. The relatively light winds associated with the near-surface air (red trajectory) originate in the vicinity of Danhauser, Newcastle as well as the vicinity of Vryheid (blue trajectory). The stronger southerly winds associated with the higher-surface air (green trajectory) originate in the vicinity of Greytown. Similarly it is noteworthy that the higher-surface (green trajectory) air flows directly over the Eskom Majuba Power Station prior to arriving at Ezamokuhle.

Figures 86 & 89 illustrate the 24-hour back trajectory results calculated for 22nd July 2020. The distinguishing feature in terms of the source region of air masses is that all the trajectories (red, blue and green) originate from an easterly direction. There is evidence of relatively light winds associated with the near-surface air (red & blue trajectories) originating in a close vicinity of Eswatini and stronger southerly winds associated with the higher-surface air (green trajectory) originating in a close vicinity of the Kwa-Zulu Natal provincial border.

The pattern of the 24-hour back trajectory results for the 17th; 21st and 22nd July 2020 (Figure 84 to 89) correspond to the influence of a semi-permanent sub-tropical anticyclone over the Highveld region. These high pressure systems are associated with large-scale subsidence which has a considerable influence on the accumulation of trace gases and aerosols in the troposphere (Garstang et al., 1996; Swap and Tyson, 1999). Held et al. (1996) showed the ridging anticyclone to result in a recirculation path that loops to the north of the Highveld region in winter (Figure 90) and to the east and south of the Highveld region in summer due to the seasonal north-south shift of the anticyclonic high-pressure belt. They dominate in mid-winter with a frequency of 80% and occur with a frequency of 20% in summer (Garstang et al., 1996).

The pollutants emitted in the Highveld region are recirculated at different spatial and temporal scales depending on the strength of the ridging anticyclone. The recirculation may be limited to the Highveld region for a few days only, or for a number of days resulting in increases in ambient pollutant concentrations. Recirculation on larger spatial scales may transport pollutants emitted in the Highveld well beyond its boundaries and into neighbouring municipalities and even across international borders (DEFF, 2010).

4.5.5 Limitations of the HYSPLIT Model

Back trajectory analysis has many sources of error and uncertainties as meteorological fields are known to fluctuate continually in time and space and are sometimes inadequately represented by a field defined at fixed locations and at fixed temporal intervals. It must be remembered that back trajectories only offer an estimate of air movement. Thus, the primary application of trajectories should be a diagnostic tool used to evaluate the flow field at different atmospheric levels (Heffter, 2002). However, trajectories based on meteorological data that are routinely available are reasonably accurate under normal atmospheric conditions (Merrill et al., 1986).

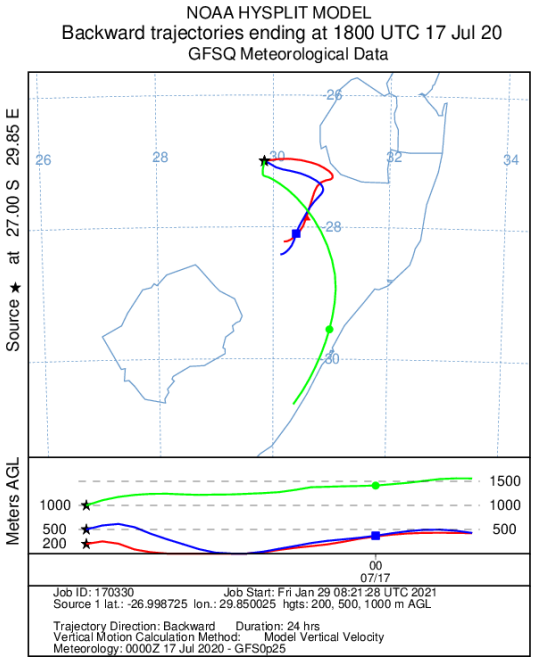

Figure 84: 24-hour back trajectory HYSPLIT model results for 17th July 2020. Trajectories originating at 200m are red; 500m, blue and 1000m, green

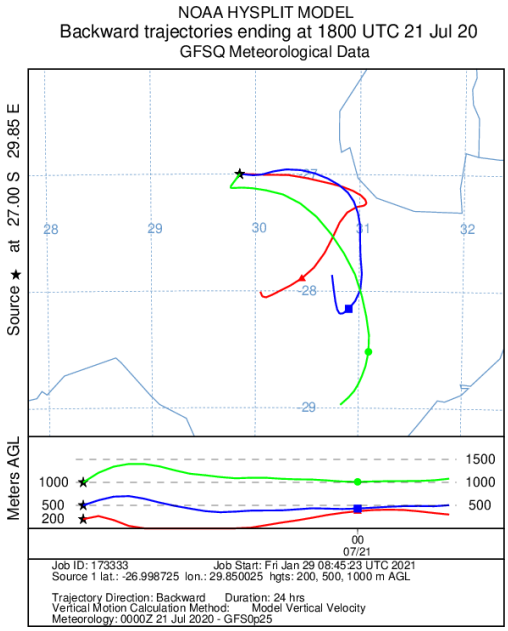

Figure 85: 24-hour back trajectory HYSPLIT model results for 21st July 2020. Trajectories originating at 200m are red; 500m, blue and 1000m, green

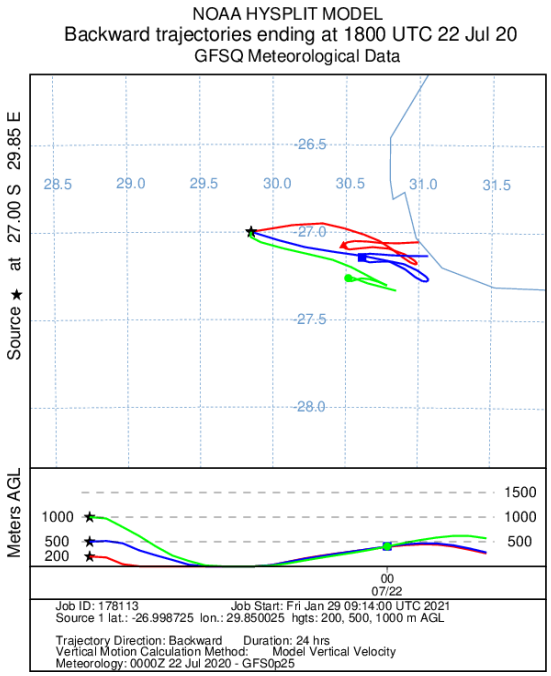

Figure 86: 24-hour back trajectory HYSPLIT model results for 22nd July 2020. Trajectories originating at 200m are red; 500m, blue and 1000m, green

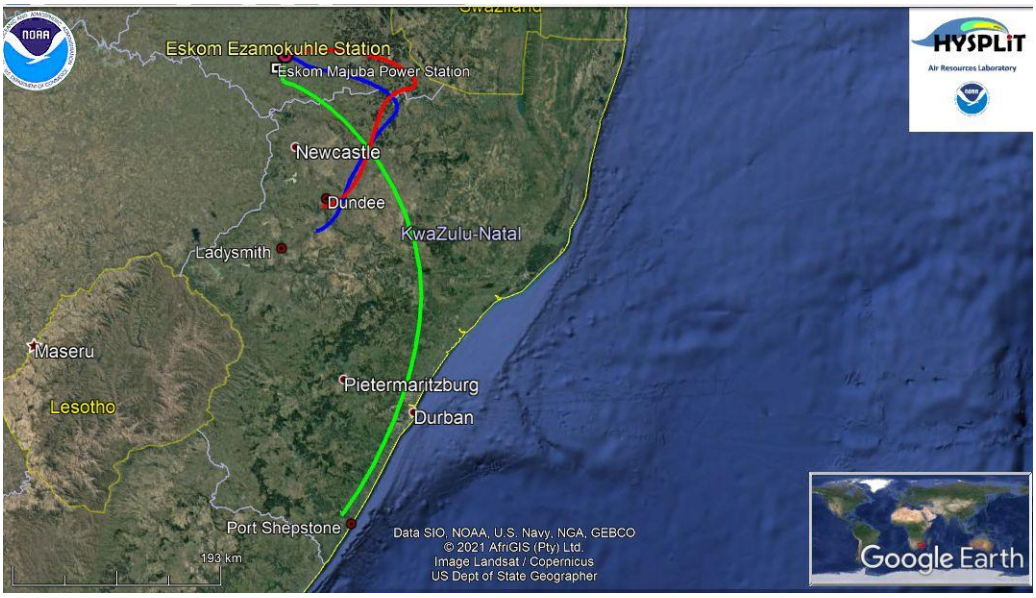

Figure 87: 24-hour back trajectory HYSPLIT model results for 17th July 2020. Trajectories originating at 200m are red; 500m, blue and 1000m, green

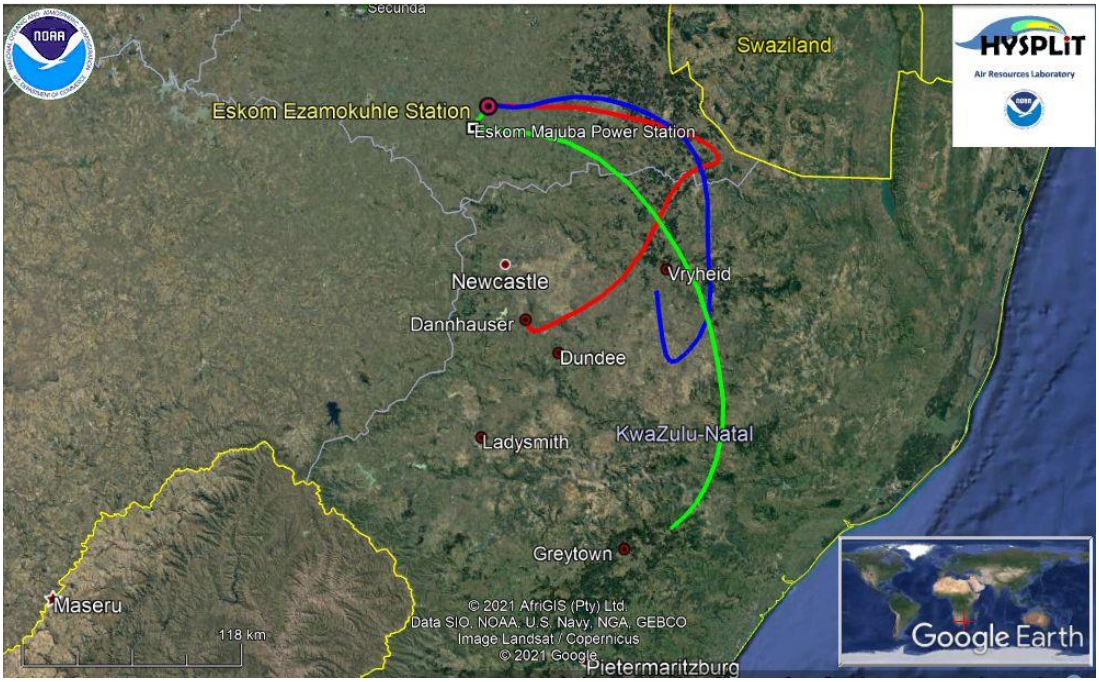

Figure 88: 24-hour back trajectory HYSPLIT model results for 21st July 2020. Trajectories originating at 200m are red; 500m, blue and 1000m, green

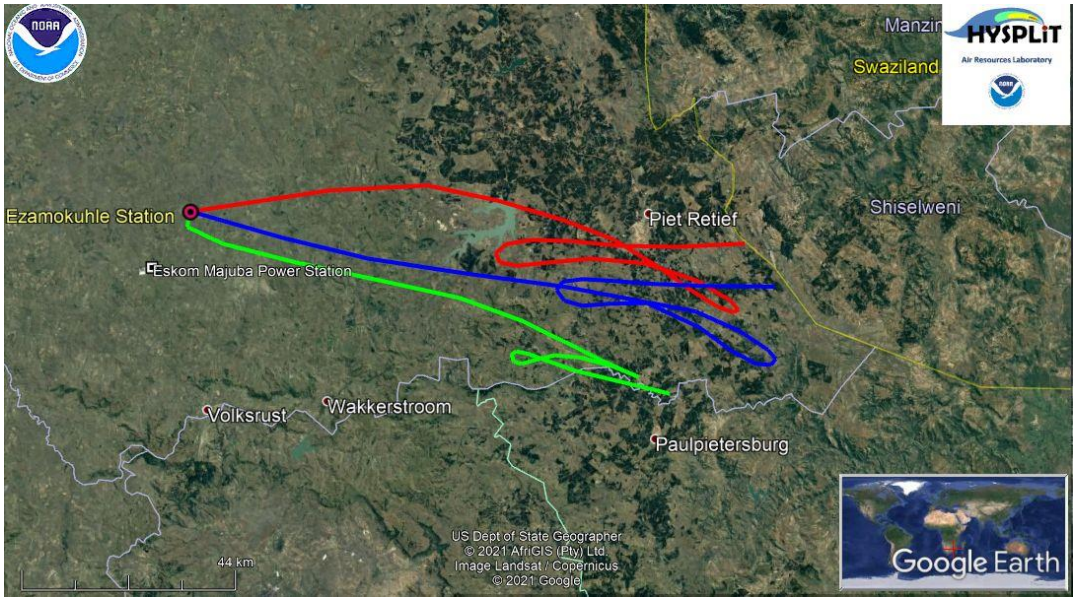

Figure 89: 24-hour back trajectory HYSPLIT model results for 22nd July 2020. Trajectories originating at 200m are red; 500m, blue and 1000m, green

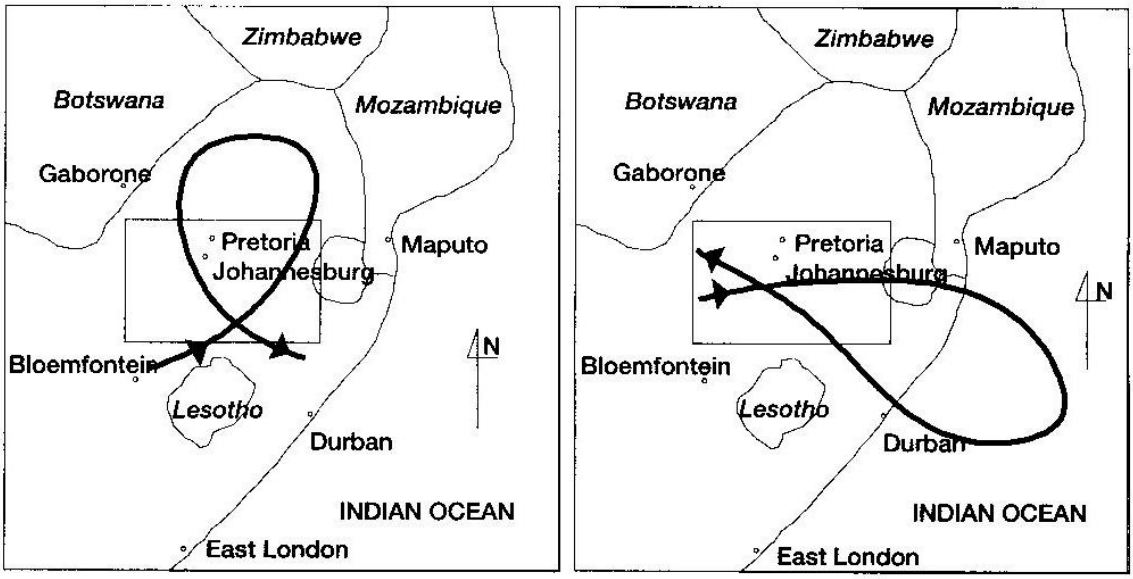

Figure 90: Characteristic wind paths during strong anticyclonic ridging from May to June (left) and August to April (right) (Held et al., 1996)

4.6 DEposition of Biogeochemically Important Trace Species (DEBITS)

Atmospheric constituents follow a series of steps from the time of their introduction into the atmosphere until their eventual removal from it. The main processes that comprise the atmospheric pathway are emissions, transformation, transport and deposition (Figure 91). Understanding the atmospheric pathways of important species and quantifying the flux of material along these pathways is fundamental to accurately determining ambient pollution concentrations in the atmosphere (Fourie, 2006).

Hence long-term research on deposition provides critical information on natural and anthropogenic influences on the atmosphere and provides information on the temporal and spatial evolution of atmospheric chemistry. Although atmospheric deposition is not measured at Ezamokuhle, long-term research on deposition measurements has been conducted at Amersfoort as part of the DEBITS programme. Due to the close spatial proximity of these two areas, the measured DEBITS Amersfoort data is likely to be a fair & representative proxy for the Ezamokuhle area.

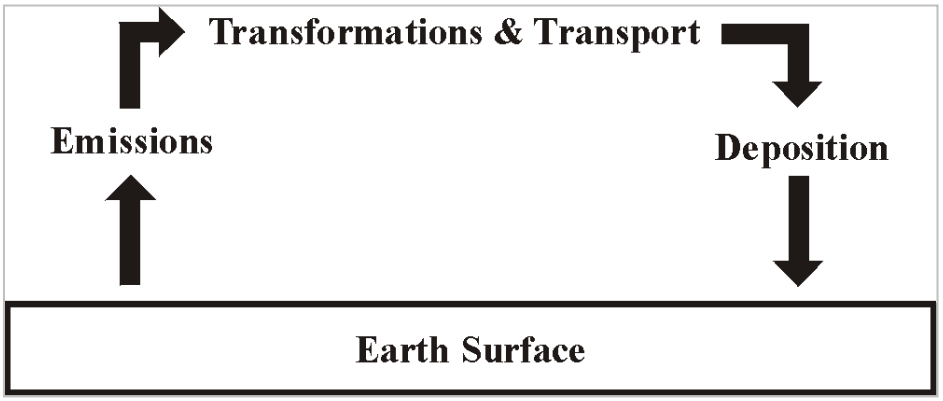

Figure 91: Schematic presentation of the atmospheric cycle and its component processes (Source: Fourie, 2006)

4.6.1 DEBITS PROGRAMME

The Deposition of Biogeochemical Important Trace Species (DEBITS) project is an international project and was established as a long-term initiative to measure atmospheric pollutants. It is a joint initiative of the International Global Atmospheric Chemistry (IGAC) programme and the World Meteorological Organisation (WMO). The main objectives of this project are to monitor the removal rates (e.g. dry and wet deposition processes) of biogeochemically important trace species and to determine which factors (e.g. physical or chemical) control deposition fluxes. Protocols and

guidelines were designed for the quality control of the experiments and analyses for all the DEBITS stations (Galy-Lacaux et al., 2003).

In South Africa, atmospheric gaseous and aerosol species are collected at five regionally representative background sites. These sites include Amersfoort, Louis Trichardt, Skukuza and Vaal Pukke which are presented within a regional context in Figure 92. With the exception of Vaal Pukke that is situated within a highly industrialised region, the DEBITS sites can be considered to be regional background sites. Atmospheric measurements at these sites are currently the most comprehensive long-term measurement dataset available for the wet and dry deposition of chemical atmospheric species in southern Africa (Martins, 2009).

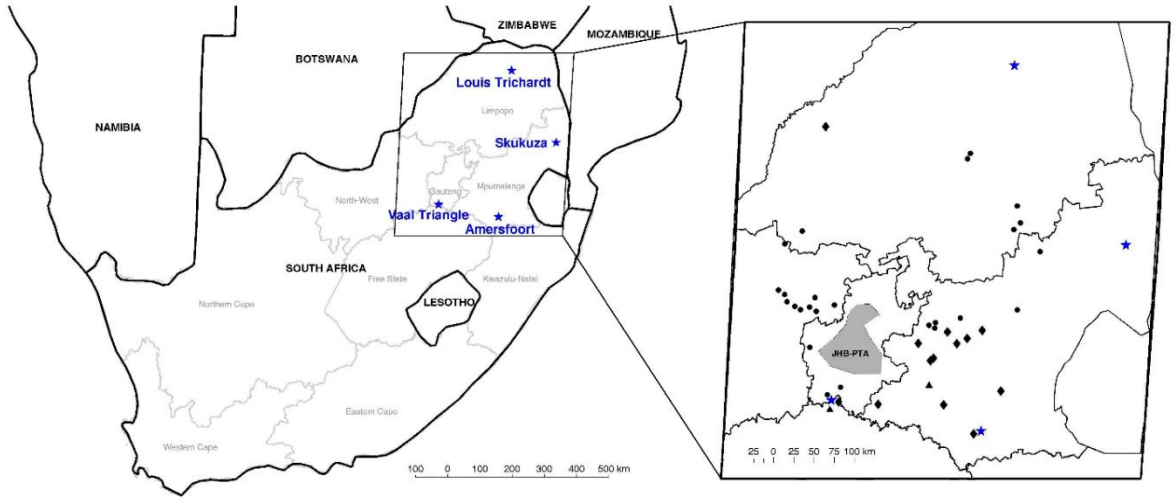

Figure 92 Locations of the DEBITS sites (DEBITS sites are indicated with a star, petrochemical industries with a triangle, coal-fired power stations with a diamond and pyrometallurgical industries with a circle) (Maritz, 2013)

4.6.2 DEBITS AMERSFOORT MEASUREMENTS

Both dry and wet deposition measurements were conducted at DEBITS Amersfoort site.

DRY DEPOSITION MEASUREMENTS

Dry deposition measurements of gases and particulates were carried out by monitoring the monthly mean concentrations of SO_2, NO_2, NH_3, HNO_3, and O_3 by conducting passive sampling. Dry deposition of gaseous species were estimated based on inferential modelling for different land use categories. Dry deposition of particles was estimated from measurements in two size fractions ($PM_{2.5}$ and PM_{10}) by sampling air on filters with Mini-Vol samplers and using standardised chemical

analysis. Aerosol sampling was conducted once a month for 24 hours at each site (Van Zyl *et al*., 2016).

WET DEPOSITION MEASUREMENTS

Wet deposition measurements were performed according to a standardised rainwater sampling, preservation and chemical analysis procedure as described by the World Meteorological Organisation (WMO).

4.6.3 DEBITS AMERSFOORT RESULTS

4.6.3.1 BACK TRAJECTORY ANALYSIS

For Amersfoort 96-hour overlay back trajectories were calculated for 2009 and 2010. Figure 93 presents the composite trajectory analysis for this period which clearly demonstrate the general anti-cyclonic recirculation pattern of air masses over this part of southern Africa (Van Heerden & Taljaard, 2015). These results corresponds to the back trajectory anlaysis (section 4.5) that was conducted in this study. Additionally Figure 93 also indicates the impact of marine air masses at Amersfoort.

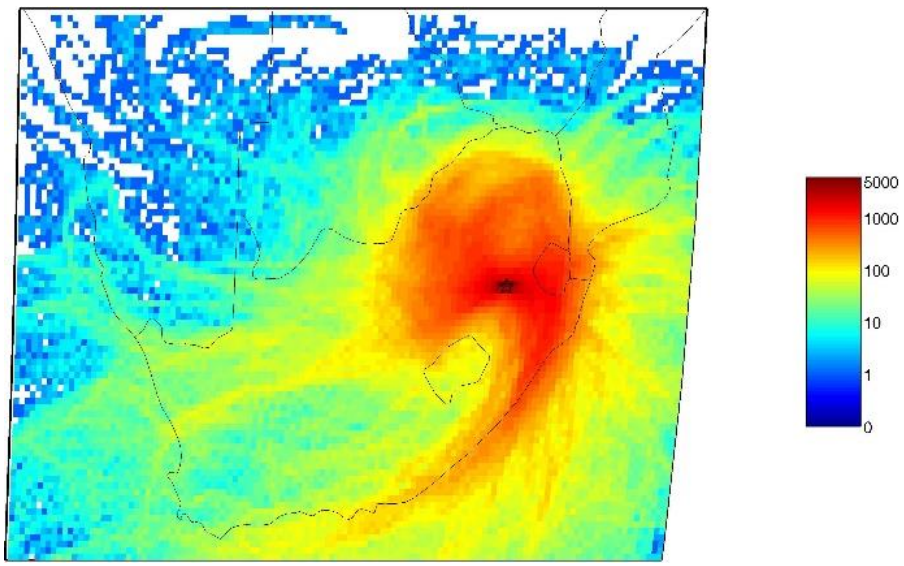

Figure 93: Back trajectory analyses for air masses arriving at Amersfoort

4.6.3.2 DRY DEPOSITION

At the Amersfoort site, there is a steady decrease in the annual average SO_2 and NO_2 concentrations up until 2004 and 2002 respectively (Figure 94 & 95). This is then followed by general increase in SO_2 and NO_2 concentrations due to increased anthropogenic activities and population growth with an associated increase in energy demand (Van Zyl et al., 2016).

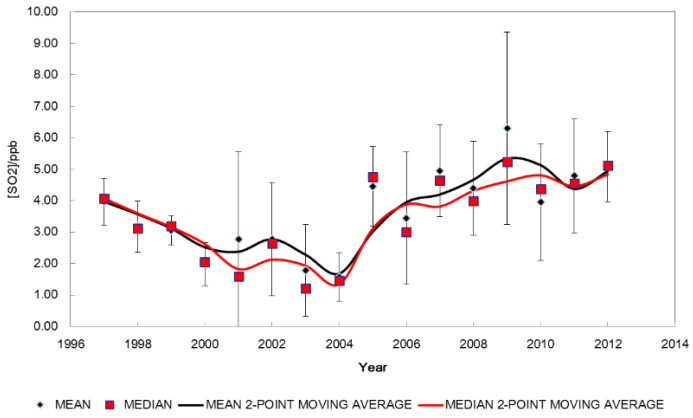

Figure 94: Annual average SO_2 concentrations measured at Amersfoort

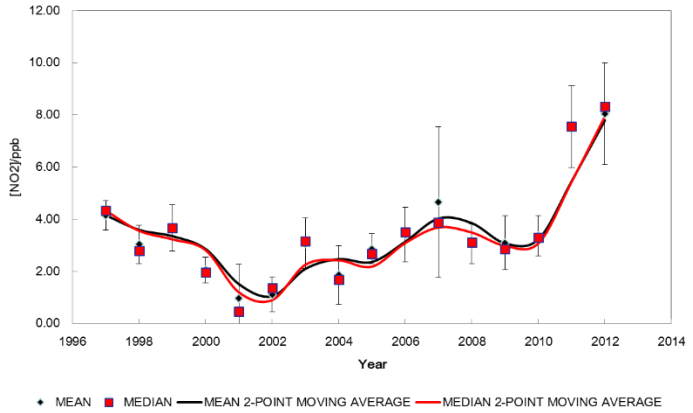

Figure 95: Annual average NO_2 concentrations measured at Amersfoort

4.6.3.3 WET DEPOSITION

Figure 96 illustrates the inter-annual variation of rainfall depth measured at the Amersfoort site for the period 2009 to 2014. The rainfall pattern is influenced by the season with most precipitation occurring between mid-spring and early autumn. The pH frequency distributions for the Amersfoort site is presented in Figure 95. The pH of individual rain events shows large fluctuations compared to the average pH values at each of the sites. However, results indicate that the pH of 99% of all rain events at Amersfoort were below 5.6 (the natural pH of rain water). The largest number of rain

events had pH values ranging between 4.0 and 4.4 at Amersfoort. Figure 95 also shows that 16.5% of rain events at Amersfoort were below 4.0.

Comparison of the frequency distribution of rainfall pH values to the previous periods reported by Mphepya et al. (2004; 2006) indicates more rain events with lower pH values for the 2009 to 2014 period, i.e. pH values at all three sites shifting towards lower pH values. These shifts towards more rain events with lower pH values could also be ascribed to a significant increase in anthropogenic activities and population growth in this part of South Africa with an associated increase in energy demand (Van Zyl, 2016).

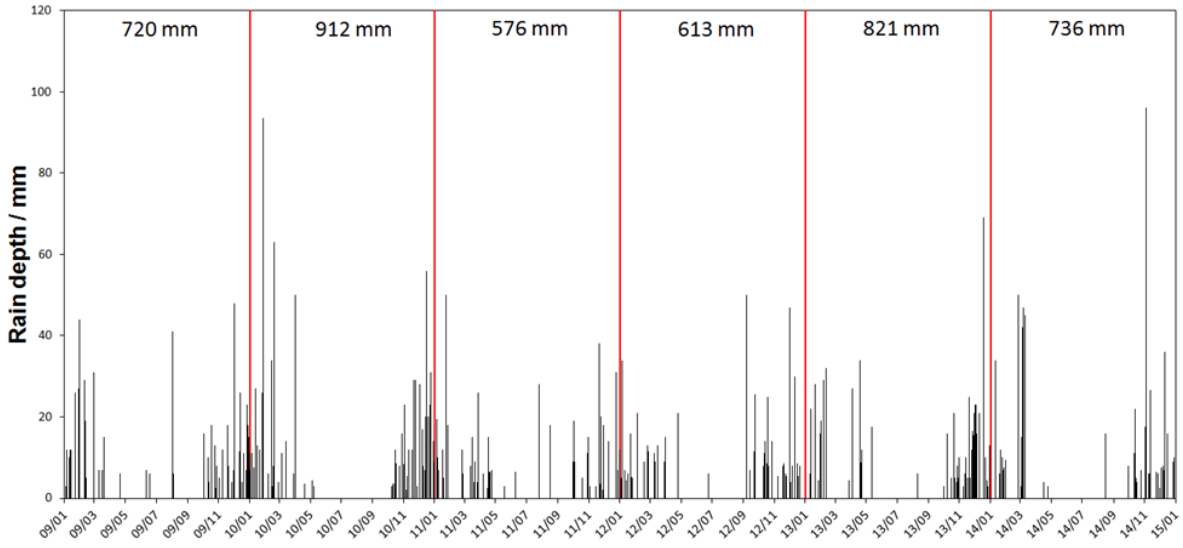

Figure 96: Precipitation events at Amersfoort occurring during the period 2009 to 2014. The annual rainfall depth for each year is indicated on the top of each figure

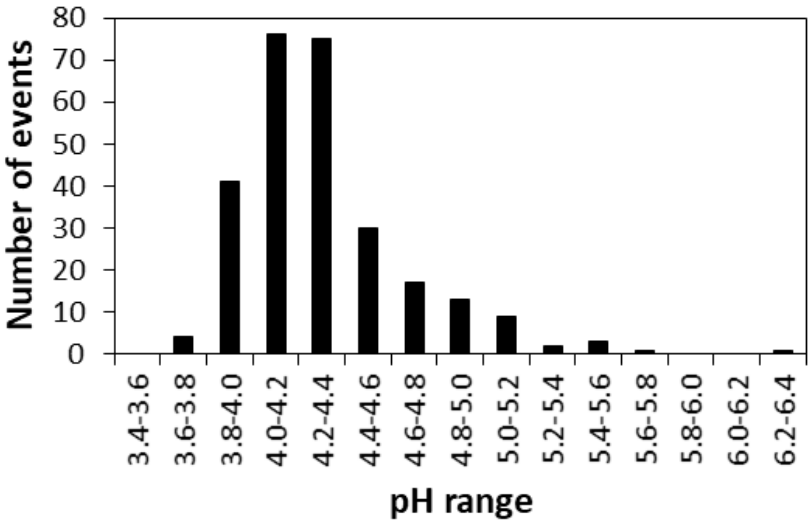

Figure 97: pH event distribution graphs for 2009 to 2014 measured at Amersfoort

5 CONCLUSION

Performed analysis of trends, correlations and general relations was based on collected measurement data obtained from three of the air quality monitoring stations (includiing both pollutant concentrations and meteorology). The findings show that for the the exceedances of the hourly NAAQS at SO_2 the Eskom Ezamokuhle and Eskom Majuba stations are attributable to the impact of an elevated tall stack emission source. Conversely the particulate matter NAAQS exceedances recorded at Eskom Ezamokuhle and Eskom Majuba stations are attributable to residential fuel burning sources. There were no recorded exceedances of the hourly NO_2 NAAQS standard.

Back trajectory modelling results has shown the transboundary impact of pollutants, within a 24-hour window, air masses from far afield such as Kwa-Zulu Natal and Eswatini impact on the Ezamokuhle airshed. The DEBITS data indicate that there is a shift towards higher deposition loading & more acidic rain events for the area which is ascribed to a significant increase in anthropogenic activities and population growth.

In summary the results of this study has demonstrated that for Ezamokuhle air quality station: the elevated SO_2 and NO_2 levels in winter; the SO_2 18:00 peak in winter; the bi-modal particulate matter peak and the elevated particulate matter concentrations during early winter months to early spring are all attributable to residential fuel burning. Hence there is an opportunity herein to reduce human

exposure to harmful levels of air pollution by reducing emissions from residential burning. Thus supporting the roll-out of Eskom's PMV air quality offset intervention project in Ezamokuhle.

6 ACKNOWLEDGEMENTS

Air Resource Management would like to thank the following individuals for their assistance in this study

- Ms Bontle Moiloa for timeously providing the team with the ambient air quality monitoring data for the Eskom Majuba and Ezamokuhle stations;
- Mr Motshewa Matimolane, Mr Bryan McCourt & Mr Maluta Mbedzi for their technical comments on the Activity 1 Method Statememt and
- Ms Khosi Mkongi for facilitating effective enagements with the wider Eskom team.
- Prof Paul Beukes and Prof Pieter van Zyl, for providing us with DEBITS publications and conference proceedings.

7 REFERENCES

1. S. Munir, T. M. Habeebullah, A. M. F. Mohammed, E. A. Morsy, M. Rehan, and K. Ali, "Analysing PM2.5 and its association with PM10 and meteorology in the arid climate of Makkah, Saudi Arabia," Aerosol and Air Quality Research, vol. 17, no. 2, pp. 453–464, 2017.

2. J. Hu, Y. Wang, Q. Ying, and H. Zhang,2014. "Spatial and temporal variability of PM2.5 and PM10 over the north China plain and the Yangtze River Delta, China," Atmospheric Environment, vol. 95, pp. 598–609, 2014.

3. Doucet, P., Sloep, P.B. 1992. "Mathematical Modeling in the Life Sciences", King's College, London,1992

4. Tiwary, A., Colls, J. "Air Pollution: Measurement, Modeling, and Mitigation", 3rd Edition, Routledge,New York, 2010

5. Carslaw D.C., Ropkins K. 2012. "Openair – an r package for air quality data analysis". Environmental Modelling and Software, pp27–28: pp52–61

6. Appel, K.W., Gilliam, R.C., Davis, N., Zubrow, A., and Howard, S.C., 2011. "Overview of the atmospheric model evaluation tool (amet) v1.1 for evaluating meteorological and air quality models".

Environmental Modelling and Software ,Vol 26 (4), pg434-443. http://www.sciencedirect.com/science/article/pii/S1364815210002653

7. Carslaw, D. “The Openair Manual Open-Source Tools for Analysing Air Pollution Data”, King’s College, London, 2015.

8. Czernecki B., Pólrolniczak M., Kkolendowicz L., Marosz M., Kendzierski S., Pilguj N. 2016. “Influence of the Atmospheric Conditions on PM10 Concentrations in Poznan, Poland”. Journal of Atmospheric Chemistry,vol 74(1),pp. 1-25. View at: https://www.researchgate.net/publication/308477377_Influence_of_the_atmospheric_conditions_on_PM10_concentrations_in_Poznan_Poland

9. Crilley L.R., Lucarelli F., Bloss W.J., Harrison R.M., Beddows D.C., Calzolai G., Navab S., Vallid G., Bernardonid V., Vecchi R. 2017. “Source apportionment of fine and coarse particles at a roadside and urban background site in London during the 2012 summer ClearfLo campaign”. Environmental Pollution 220: pp766–778

10. Pattinson W., Kingham S., Longley I., Salmond J. 2016. “Potential Pollution Exposure Reductions from Small-Distance Bicycle Lane Separations”. Journal of Transport & Health,Vol 4,pp40-52. View at: https://www.sciencedirect.com/science/article/abs/pii/S2214140516303504

11. Salvador P., Alonso-Pérez S., Pey J., Artíñano B., Debustos J.J., Alastuey A., Querol X. 2014. “African dust outbreaks over the western Mediterranean Basin: 11-year characterization of atmospheric circulation patterns and dust source areas”. Atmospheric Chemistry and Physics Vol 14(13): pp6759–6775. View at: https://www.researchgate.net/publication/263036412_African_dust_outbreaks_over_the_western_Mediterranean_Basin_11-Year_characterization_of_atmospheric_circulation_patterns_and_dust_source_areas

12. Schweizer D.,and Cisneros R. 2014. “Wildland Fire Management and Air Quality in the Southern Sierra Nevada: Using the Lion Fire as a case study with a multi-year perspective on PM2.5 impacts and fire policy”. Journal of Environmental Management Vol 144: pp 265–278. View at: https://www.sciencedirect.com/science/article/pii/S0301479714003089?via%3Dihub

13. Crilley L.R., Bloss W.J., Yin J., Beddows D.C., Harrison R.M., Allan J.D., Young D.E., Flynn M., Williams P., Zotter P., Prevot A.S.H., Heal M.R., Barlow J.F.,Halios C.H., Lee J.D., Szidat S., Mohr

C., Prevot A.S. 2015. “Sources and contributions of wood smoke during winter in London: Assessing local and regional influences”. Atmospheric Chemistry and Physics Vol 15(6): pp 3149–3171. View at: https://acp.copernicus.org/articles/15/3149/2015/

14. Jang E., Do W., Park,G., Kim M., Yoo E. 2016. “Spatial and temporal variation of urban air pollutants and their concentrations in relation to meteorological conditions at four sites in Busan, South Korea”. Atmospheric Pollution Research Vol 8(1): pp 89–100. View at: https://www.sciencedirect.com/science/article/abs/pii/S1309104216301192?via%3Dihub

15. Szulecka,A., Oleniacz R , and Rzeszutek,M. 2017. “Functionality of Openair Package in Air Pollution Assessment and Modeling — A Case Study of Krakow”. Environmental Protection and Natural Resources,Vol 28(2):pp 22-27. View at: https://content.sciendo.com/view/journals/oszn/28/2/article-p22.xml?language=en&tab_body=abstract

16. Malby, A.R., Whyatt, J.D., and Timmis, R.J. 2013. “Conditional Extraction of Air-Pollutant Source Signals from air-quality monitoring”. Atmospheric Environment, Vol 74(2013):pp 112-122

17. Carslaw, D.C.,and Carslaw, N., 2007. “Detecting and characterising small changes in ur-ban nitrogen dioxide concentrations”. Atmospheric Environment Vol 41(22): pp 4723-4733.View at: http://dx.doi.org/10.1016/j.atmosenv.2007.03.034

18. Malby, A.R., Timmis, R.J., Whyatt, J.D., 2008. “Combining modelling and monitoring to Estimate Fugitive Releases from a Heavily-Industrialised Site”. Proceedings from the 12th Conference on Harmonisation within Atmospheric Dispersion Modelling for Regulatory Purposes (HARMO 12), Cavtat, Croatia,October 6-9, 2008, pp. 939-943. View at: http://www.harmo.org/Conferences/ Cavtat/12harmo.asp

19. Shu,M., Dang,D., Nguyen,T., Hsu,B., and Pham,K. 2017. “The application of bivariate polar plots and k-means clustering to analysis air pollution in Taoyuan, Taiwan”. International Journal of Advance Engineering and Research Development, Vol 4(4),pp 553-557

20. Carslaw, D.C., Beevers, S.D., Ropkins, K., Bell, M.C., 2006. “Detecting and quantifying aircraft and other on-airport contributions to ambient nitrogen oxides in the vicinity of a large international airport”. Atmospheric Environment 40 (28),pp 5424-5434. View at: https://www.sciencedirect.com/science/article/abs/pii/S1352231006004250?via%3Dihub

21. Westmoreland, E.J., Carslaw, N., Carslaw, D.C., Gillah, A., and Bates, E., 2007. “Analysis of air quality within a street canyon using statistical and dispersion modelling techniques”. Atmospheric Environment, Vol 41(39), pp 9195-9205. View at: https://doi.org/10.1016/j.atmosenv.2007.07.057

22. Carslaw D.C., and Beevers S.D. 2013. “Characterising and understanding emission sources using bivariate polar plots and k-means clustering”. Environmental Modelling and Software, Vol 40: pp 325–329. View at: https://doi.org/10.1016/j.envsoft.2012.09.005

23. Jones, A.M., Harrison, R.M., Baker, J., 2010. “The wind speed dependence of the concentrations of airborne particulate matter and nox”. Atmospheric Environment Vol 44(13), pp 1682-1690. View at:http://www.sciencedirect.com/science/article/B6VH3-4Y7P72C-2/2/f6c65e5f49ac3e9862d4c1803d4735c0.

24. Tellaetxe, I.U., and Carslaw, D.C. “Conditional bivariate probability function for source identification”,Environmental Modelling & Software,Vol 59,pp 1-9. View at: https://www.sciencedirect.com/science/article/pii/S1364815214001339?via%3Dihub

25.Thangprasert, N.,and Suwanarat,S. 2017. “The Relationships between Wind Speed and Temperature Time Series in Bangkok, Thailand. Journal of Physics: Conference Series, 901 (2017) 01204. View at: https://iopscience.iop.org/article/10.1088/1742-6596/901/1/012043

26. Grundstrom, M., Tang, L., Hallquist, M., Nguyen, H., Chen, D., and Pleijel,H. “Influence of atmospheric circulation patterns on urban air quality during the winter” Atmospheric Pollution Research,Vol 6(2), pp 278-285. View at: https://doi.org/10.5094/APR.2015.032.

27. Garstang, M., Tyson, P.D., Swap, R., Edwards, M., Kållberg, P. and Lindesay, J.A. (1996). Horizontal and vertical transport of air over Southern Africa. Journal of Geophysical Research, 101 (D19), 23721-23736.

28. Swap, R., Garstang, M., Macko, S.A., Tyson, P.D., Maenhaut, W., Artaxo, P., Kallberg, P. and Talbot, R. (1996). The long-range transport of southern African aerosols to the tropical south Atlantic. Journal of Geophysical Research, 101 (D19), 23777-23791.

29. Held, G., Gore, B.J., Surridge, A.D., Tosen, G.R. and Walmsley, R.D. (eds) (1996), Air Pollution and its Impacts on the South African Highveld, Environmental Scientific Association, Cleveland, 144 pp.

30. DEFF (2010), Air Quality Baseline Assessment for the Highveld Priority Area

31. Merrill, J.T., Bleck, R. and Boudra, D.B. (1986). Techniques of Lagrangian trajectory analysis in isentropic coordinates. Monthly Weather Review, 114, 571-581.

32.Lacaux J.P (2003), IGACtivities Newsletter, issue no.27, January 2003, (http://www.igac.noaa.gov/newsletter/igac27/Jan_2200_IGAC_27.pdf)

33. Martins J.J, Dhammapala R.S, Lachmann G, Galy-Lacaux C and Pienaar J.J., (2007): 'Long-term measurements of sulphur dioxide, nitrogen dioxide, ammonia, nitric acid and ozone in southern Africa using passive samplers", South African Journal of Science, 103, 1-7

34. Mphepya J.N. 2004, 'Precipitation Chemistry in Semi-Arid Areas of Southern Africa: A Case Study of a Rural and an Industrial Site', Journal of Atmospheric Chemistry 47: 1–24.

36. Van Zyl, P.G., Conradie, E.H., Pienaar, J.J., Beukes, J.P., Galy-Lacaux, C., Swartz, J., Liousse, C., and Mkhatshwa, G.V., An assessment of precipitation chemistry at the South African DEBITS sites, 13th Quadrennial Symposium of the International Commission on Atmospheric Chemistry and Global Pollution, (iCACGP) 13th Science Conference of the International Global Atmospheric Chemistry Project, (IGAC), Natal Convention Center (NCC), Natal, Brazil 22-26th September 2016

37. Van Zyl, P.G., Beukes, J.P.;Conradie, E.H.; Pienaar, J.J.; Mkhatshwa, G.; Fourie, G.D. and Galy-Lacaux, C., Deposition measurements in southern Africa, Workshop on Atmospheric Depostion Processes, The Abdus Salam International Centre for Theoretical Physics, Trieste, Italy, 21-25 May 2012.

38. P. Maritz, J.P. Beukes, P.G. van Zyl, E.H. Conradie, A.D. Venter, J.J. Pienaar, C. Liousse, C. Galy-Lacaux, Spatial and temporal assessment of atmospheric organic and black carbon concentrations at South African DEBITS sites, 16th International Union of Air Pollution Prevention Association (IUAPPA) Congress, 29 September – 4 October 2013, International Convention Centre, Cape Town, South Africa.